Master's Theses and Capstones   Student Scholarship

Spring 2013

Observations of pockmark flow structure in Belfast Bay, Maine

Christina L. Fandel
University of New Hampshire, Durham

Follow this and additional works at: https://scholars.unh.edu/thesis

Recommended Citation

OBSERVATIONS OF POCKMARK FLOW STRUCTURE

IN BELFAST BAY, MAINE

BY

CHRISTINA L. FANDEL
BS, College of Charleston, 2010

THESIS

Submitted to the University of New Hampshire
in Partial Fulfillment of
the Requirements for the Degree of

Master of Science
in
Earth Sciences: Ocean Mapping

May, 2013

UMI Number: 1523791

UMI

Dissertation Publishing

UMI 1523791

ProQuest
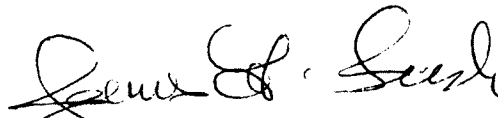
This thesis has been examined and approved.

Thesis Director
Thomas C. Lippmann
Research Associate Professor of Earth Sciences and Ocean
Engineering

Diane L. Foster
Associate Professor of Mechanical Engineering and Ocean
Engineering

James D. Irish
Research Professor of Ocean Engineering

Larry A. Mayer
Professor of Ocean Engineering and Marine Sciences
and Earth Sciences

11 April 2013
Date

DEDICATION

This thesis is dedicated to John Fandel, my father, whose compassion, support, and diligence has shaped me into the person I am today and Maggi Fandel, my mother, whose candor and vivacious personality have taught me not to lose sight of the lighter things in life.

ACKNOWLEDGEMENTS

TABLE OF CONTENTS

LIST OF TABLES

LIST OF FIGURES

ABSTRACT

OBSERVATIONS OF POCKMARK FLOW STRUCTURE IN BELFAST BAY, MAINE

by

Christina L. Fandel
University of New Hampshire, May, 2013

Vertical current and CTD profiles were acquired over a small, spherical pockmark and a larger, more elongated pockmark in Belfast Bay, Maine in July 2011. These observations showed evidence for mixing within the pockmarks, a rotational pattern that resembles open cavity flow, and incipient motion along the rims. Over the center of each pockmark, observations of uniform temperature properties below 12 m are indicative of mixing within the pockmark. The observed complex rotational structure over each pockmark shows significant rotation with depth and a greater degree of rotation during ebbing tide. These observations are qualitatively consistent with circulation patterns predicted by cavity flow models. Critical Shields parameters for cohesive sediment were estimated at the rim and center of each pockmark and were only exceeded along the rim. During the infrequently observed upwelling events, and in the absence of flocculation, suspended sediment would be unable to settle through the water column.

TABLE OF SYMBOLS

Variable	Symbol
Sediment shape factor, relates drag force acting on particle to drag force acting on sphere of equivalent volume	b_1
Sediment shape factor, describes platiness of particle	b_2
Pockmark relief (m)	D
Vorticity thickness (m)	δ_w
Median grain diameter (m)	d_{50}
Grain diameter (m)	d_n
Maximum grain diameter (m)	$d_{n_{max}}$
Acceleration due to gravity (m/s^2)	g
Ratio of cohesive force acting in vertical relative to submerged weight of grain	$\dfrac{F_A}{F_s}$
Nikuradse roughness	k_s
Pockmark diameter (along major axis) (m)	L
Number of observations	N
Density of seawater (kg/m^3)	ρ
Density of sediment (kg/m^3)	ρ_s
Angle of repose (deg)	φ
Characteristic aspect ratio of cylindrical grains	R
Critical particle Reynolds number	Re_*

Variable	Symbol
Shields parameter	θ
Critical Shields parameter	θ_{cr}
Skill	S
Bed shear stress (Pa)	τ_b
Yield stress (N/m^2)	τ_y
Current magnitude (m/s)	U
Horizontal component of the velocity at the bed (m/s)	U_1
Horizontal component of the freestream velocity (m/s)	U_2
East-West horizontal component of velocity (positive East) (m/s)	u
Friction velocity (m/s)	u_*
Critical friction velocity (m/s)	u_{*cr}
Dynamic viscosity of seawater $(Pa\ s)$	μ
North-South horizontal component of velocity (positive North) (m/s)	v
Terminal settling velocity (m/s)	V_s
Water content $(\%)$	W
Vertical velocity (positive Up) (m/s)	w
Kinematic viscosity of seawater (m^2/s)	v
Vertical direction (positive up, z = 0 at bed) (m)	z
Roughness length (m)	z_o

CHAPTER 1

INTRODUCTION

1.1 Belfast Bay

Penobscot Bay is situated along the central coast of Maine and is the largest estuarine embayment within the Gulf of Maine. Regional circulation is driven by tidal currents that are modified by wind-driven stress at the surface. Located within the northwestern quadrant of Penobscot Bay, Belfast Bay comprises a shallow (< 70 *m*), muddy environment that is fed by the Passagassawakeag River to the northwest and the Penobscot River to the northeast. Seafloor topography in Belfast Bay is riddled with hundreds of large, spherical to elongated depressions, referred to as pockmarks.

Andrews et al., 2010 simultaneously acquired backscatter, bathymetric, and seismic-reflection data within a 25 km^2 region of Belfast Bay in 2006. The surveyed area ranged in depth from 7 to 49 *m* and consisted of an estimated 1,767 pockmarks. Pockmark morphology in Belfast Bay transitions from more spherical in the northern region to more elongated further south where the bay significantly constricts in size. This morphological transition to a more elongated shape with progression south is a characteristic that is also observed in other regional pockmark fields (*e.g.* Blue Hill Bay, ME; Passamaquoddy Bay, New Brunswick, Canada) and is suggested to be related to increased uni-directional, near-bed flow (Brothers, *et al.*, 2012).

Methane-escape from Holocene estuarine sediment has been evoked as the primarily mechanism of pockmark formation in Belfast Bay based on multiple geophysical data observations of shallow natural gas within this sediment package (Barnhardt *et al.*, 1997; Christian, 2000; Andrews *et al.*, 2010). Historical bathymetric data dating back to 1872 document the presence of multiple pockmarks within Belfast Bay and suggest that at least a portion of the field existed about 140 years ago. Furthermore, the Belfast Bay pockmarks do not protrude below the Pleistocene/Holocene unconformity and are therefore suggested to be no older than 11,000 years. The present degassing activity within Belfast Bay remains controversial with evidence existing both for (*e.g.* Kelly *et al.*, 1994; Barnhardt *et al.*, 1997) and against (Ussler *et al.*, 2003) an actively venting field. A recent pockmark presence/absence analysis of Belfast Bay indicated no change in macro-scale (> 5 *m*) pockmark frequency or distribution between the years 1999 and 2008, yet, long-term pockmark evolution and maintenance mechanisms remain uncertain. Although multiple studies have obtained geophysical data within the Belfast Bay pockmark field (*e.g.* Kelley, *et al.*, 1994; Ussler, *et al.*, 2003; Rogers *et al.*, 2006; Andrews, *et al.*, 2010), none have investigated the flow structure and circulation patterns in the vicinity of these pockmarks. Analysis of the flow and sediment dynamics around pockmarks will lead to a better understanding of micro-scale pockmark evolution in Belfast Bay as well as provide valuable insight regarding the required frequency of repeat hydrographic surveys to properly characterize the regional bathymetry.

This study examines the vertical temperature, salinity, and current structure over two pockmarks in Belfast Bay, Maine to investigate the mechanisms of long-term, post-

formation maintenance. Two pockmarks were studied: a spherical pockmark with a 45 *m* diameter and 12 *m* of relief located in 21 *m* water depth in the northern part of Belfast Bay and a more elongated pockmark with an 80 *m* diameter and 17 *m* of relief located in 24 *m* water depth in the southern region of Belfast Bay. The time-varying structure of the water column was examined by completing multiple Conductivity, Temperature, and Depth (CTD) casts over the center of each pockmark for a complete tidal cycle. Vertical current profiles were measured using bottom-mounted Acoustic Doppler Current Profilers positioned at the rim and center of each pockmark. The results of these observations are summarized within three separate papers comprising Chapters 2 - 4 of this thesis. Each chapter is comprised of an independent abstract, introduction, methods, discussion, and conclusion section.

Chapter 2 presents the majority of the survey methods used in this study as well as summarizes the overall current observations. This paper investigates the evidence for mixing within these depressions and examines the influence of roughness-induced form drag on the local flow regime. Chapter 3 examines the rotational structure observed over the sampled pockmarks and introduces a conceptual flow model that may explain near-shore, pockmark circulation patterns, specifically in Belfast Bay, Maine. Chapter 4 estimates periods of incipient motion from near-bed current observations and measured grain size characteristics. Maximum grain size estimations under terminal settling velocities are examined to infer whether or not sediment is expected to settle towards the seafloor or remain in suspension, specifically during periods of predicted incipient motion. Broad conclusions of all three studies are summarized in Chapter 5 and future research directions are discussed.

CHAPTER 2

OBSERVATIONS OF POCKMARK FLOW STRUCTURE IN BELFAST BAY, MAINE, PART 1: MIXING

2.1 Abstract

Field observations of current profiles and temperature and salinity structure were used to examine vertical mixing within two pockmarks in Belfast Bay, Maine. The morphology of the sampled pockmarks is distinctly different, the first is nearly circular in shape and located in 21 m water depth with a 45 m diameter and 12 m of relief and the other is more elongated and located in 25 m water depth with an 80 m diameter and 17 m of relief. Hourly-averaged current profiles were acquired from bottom-mounted acoustic Doppler current profilers (ADCPs) deployed on the rim and center of each pockmark over successive 42 hour periods in July 2011. CTD casts at the rim and center of each pockmark show warmer, fresher water with evidence of both active and fossil thermocline structure in the upper water column, about 5-8 m above the rim, and well-mixed water below to the bottom of each depression. Vertical velocity observations show up-welling and down-welling events that extend from above the rim and into the depths of each pockmark indicating active overturning of the water column and mixing of flow above and below the rim. An anomalous temperature rise was nearly simultaneously recorded by temperature sensors on both the rim and center ADCPs and occurs

4

coincident with an overturning event below the rim. Vertical profiles of horizontal velocities show depth variation both at the center and rim consistent with turbulent logarithmic layers, and suggests that form drag may be significantly influencing the local flow regime. Current and temperature and salinity observations obtained over the sampled pockmarks suggest active mixing and overturning within the pockmarks, and enhanced turbulence over these depressions from upstream bathymetric irregularities induced by other, distant pockmarks.

2.2 Introduction

Pockmarks are roughly conical depressions in the seafloor that are typically associated with sub-surface fluid and gas expulsion. These crater-like features are distributed in a variety of global geologic environments ranging from shallow coastal regions (*e.g.,* Brothers et al., 2011; Wildish *et al.*, 2008), to deep offshore settings (*e.g.,* Hovland and Judd, 1988; Hovland and Svensen, 2006). Pockmarks range in size from less than 1 *m* to over a kilometer in diameter and are believed to be formed by the gradual or instantaneous release of underlying gas, groundwater, or pore-water (*e.g.,* Scanlon and Knebel, 1989; Christodoulou, *et al.,* 2003).

A major source of uncertainty in pockmark research relates to age estimation and mechanisms for long-term maintenance, specifically in non-actively venting fields. Observations of the current structure as well as the physical properties of the water column within and around these depressions are needed to improve our understanding of sediment transport within pockmarks. These observations will better constrain models for age approximation and offer insight into mechanisms of post-formation pockmark

5

maintenance. In addition, many pockmark fields are associated with abundant biological communities within individual pockmarks (*e.g.*, Gay, *et al.*, 2005; Hovland, *et al.*, 2005; Ritt, *et al.*, 2011; Wildish, *et al.* 2008), and investigation of current flow in the vicinity of pockmarks will lead to more accurate estimations of faunal and nutrient distribution patterns in these seafloor depressions.

Belfast Bay is located in central Maine in the northwestern quadrant of Penobscot Bay and consists of an extensive pockmark field (Figure 2-1) (Scanlon and Knebel, 1989). Belfast Bay is characterized as a shallow 10-50 *m* deep, estuarine environment with predominant fresh-water input by the small Passagassawakeag River to the northwest and the larger Penobscot River to the northeast (USGS, 2010). Belfast Bay contains over 1,700 pockmarks within a 25 *km²* area (Andrews, *et al.*, 2010). Pockmark morphology transitions from a nearly circular shape in the shallower, northern region to a more elongated shape in the deeper, southern region. Biogenically derived methane release from Holocene estuarine mud has been identified as the primary method of pockmark formation in Belfast Bay, yet the relative degassing activity and maintenance mechanisms of the pockmarks remain unresolved (Kelley, *et al.*, 1994). Although much research has addressed pockmark formation, specifically in Belfast Bay (*e.g.*, Scanlon and Knebel, 1989; Kelley, *et al.*, 1994; Rogers, *et al.*, 2006; Brothers, *et al.*, 2012), few studies have acquired physical current or temperature measurements in the vicinity of pockmarks.

This study presents field observations of the evolution of the vertical temperature, salinity, and current structure over two pockmarks in Belfast Bay, Maine. Both

pockmarks show evidence of active mixing of water within them, and a turbulent flow structure induced by internal pockmark circulation and upstream bathymetric irregularities.
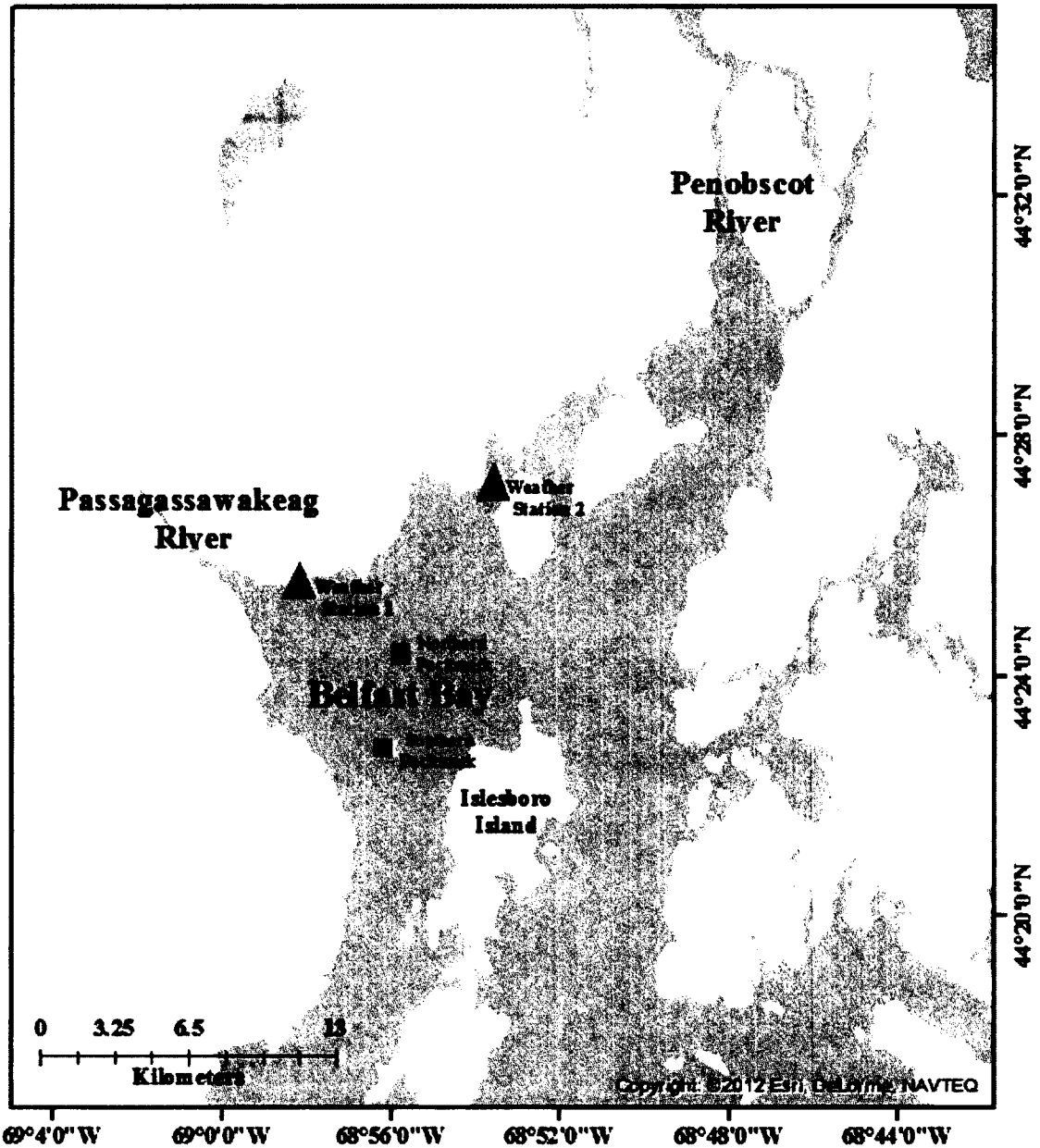
Figure 2-1. Overview map of Belfast Bay, Maine, with the approximate location of each sampled pockmark are shown by a green box. Weather stations 1 and 2 are located approximately 1.5 miles east of Belfast and Searsport, Maine, respectively and are marked by blue triangles.

2.3 Methods

Field observations of the temperature, salinity and current structure were obtained over the rim and center of two pockmarks in Belfast Bay with conductivity, temperature, and depth (CTD) casts and bottom-mounted acoustic Doppler current profilers (ADCPs). Candidate pockmarks were selected from a 5 by 5 *m* resolution bathymetric map of Belfast Bay produced from a multibeam survey conducted by the U.S. Geological Survey in cooperation with the University of Maine in 2006 and 2008 (Brothers *et al.*, 2011). Pockmarks were selected based on proximity to other pockmarks, depth restrictions of the instrumentation, and characteristic morphology. The chosen pockmarks are both located within regions of high pockmark density and consist of a spherical pockmark in 21 *m* water depth with a 45 *m* diameter and 12 *m* of relief located in the northern region of the bay and an elongated pockmark in 25 *m* water depth with a 80 *m* diameter and 17 *m* relief located to the south (Figure 2-2). The northern pockmark is located near a complex convergence zone of tidal currents flowing around Islesboro Island, whereas the southern pockmark is located in a narrower channel to the west of Islesboro Island where tidal currents are stronger and more aligned with the direction of the channel. Data were obtained in the northern pockmark from 26 July 1500 EST through 28 July 1100 EST (Julian days 207.8-209.6), and in the southern pockmark from 28 July 1700 EST through 30 July 1000 EST (Julian days 209.9-211.6) during a rising spring tide.
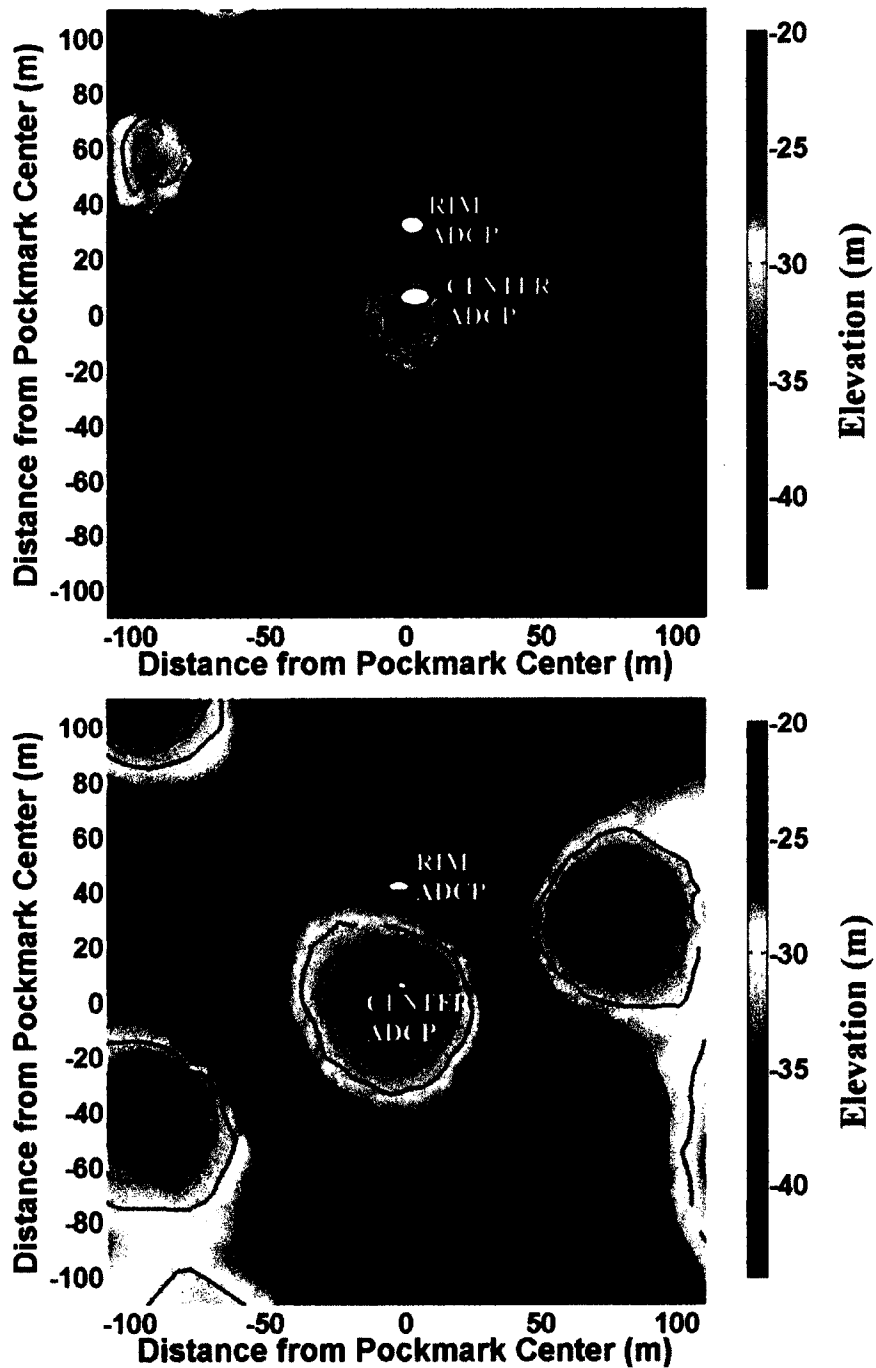
Figure 2-2. Color-filled contour plots show bathymetric data collected over the northern (upper) and southern (lower) pockmark with x and y axes showing the estimated distance from the center of each pockmark. The white dots denote the approximate location of each current meter mount along the rim and center of each pockmark with associated uncertainty denoted by the size of each dot. Elevations are referenced to mean sea level.

Wind speed, direction, and gust speed were obtained from meteorological stations located on shore near the townships of Belfast and Searsport, Maine (Weather Underground Organization, 2011) (Figure 2-1). Observations were made about 30 *m* above mean seal level at the Belfast weather station and 15 *m* above mean seal level at the Searsport weather station. Wind speed, direction and gust data were collected and distributed by Weather Underground, Inc., and averaged over 1 *hr* intervals. Although winds were variable over Belfast Bay, the general agreement between the two distant sites suggests that the length scales of the variability would not greatly influence the interpretation of our results. Wave heights were generally small, with limited swell in Penobscot Bay and with low energy (order 0.25 *m* significant wave heights), high-frequency sea waves with short periods (order 1-3 *s*) that were spun up and down by the local diurnal wind patterns.

2.3.1 Bathymetry

A high-resolution bathymetric survey was conducted over each pockmark for a complete tidal cycle by making many (of order 50) criss-crossing transects using the R/V Cocheco (Figure 2-2). Bathymetric data were acquired using a side-mounted ODOM THP 200 single-beam echo sounder operating at 200 *kHz*. Sub-meter positioning accuracy was achieved using an Omnistar 8200 HP differential GPS system that continually received differential GPS corrections via satellite transmission. Bathymetric data were post processed and gridded to 2.5 *m* resolution using Computer Aided Resource Information System (CARIS) Hydrographic Information Processing System (HIPS) 7.0 software. Tidal observations were acquired from NOAA tidal station 8418150

located to the south in Portland, Maine, and used to reference bathymetric data to the mean sea level. Temporal corrections were applied to account for the known offset in the tidal wave arrival time between Portland and Belfast.

2.3.2 Current Observation

Three-component current velocity profiles were concurrently acquired at the rim and center of each pockmark over the 48 *hr* sampling period. Upward-looking RDI Workhorse 300 *kHz* ADCPs were installed on triangular aluminum frames about 1 *m* on a side with height of 0.52 *m* and 0.63 *m* above bottom in the rim and center of the pockmarks, respectively (Figure 2-3). Velocity profiles were sampled in regularly spaced 0.5 *m* bins through the water column beginning 2.37 *m* (rim location) and 2.24 *m* (center location) above the seafloor. The ADCPs sampled currents in each bin at 1.6 *s* intervals and recorded averaged currents over 5 *min* periods. The center current meter mount additionally housed a Nortek Aquadopp acoustic current meter positioned 0.7 *m* above the seafloor that sampled at 1 *Hz* and recorded near-bed mean currents over 1 *min* periods. Currents were further averaged after data collection over 1 *hr* intervals and over 4 adjacent vertical bins to yield mean three-component current profiles with better than 0.0025 *m/s* accuracy. All ADCP and Aquadopp data were synchronized to within 1 *s* UTC during sampling.

Current meter mount locations at the center and rim of each pockmark were estimated by calculating a time-average of the recorded GPS data over a time interval within ± 2 minutes of the recorded deployment time (Figure 2-2). Rim current meter mounts were visible within single-beam echo sounder backscatter data at each pockmark

12

site and their location was approximated by obtaining a mean position from manual inspection of multiple backscatter profiles. The relative offset between the time-averaged and the backscatter-delineated position of the rim current meter mount was applied to the time-averaged position at the center and designated as the location of the center current meter mount. The associated uncertainty of each estimated ADCP location was approximated by calculating the quadratic sum of the individual uncertainty sources, and estimated to be within about +/- 3.5 m horizontally at the northern pockmark and within about +/- 1.8 m horizontally at the southern pockmark. The approximated position of the center current meter mount in both pockmarks is along the northeastern sidewall which is consistent with internally measured orientation angles recorded by the ADCPs.

Pitch and roll angles were measured internally by each ADCP with accuracy of +/- 0.5 deg. The rim ADCPs were deployed on approximately level ground, with a tilt angle of about 2 deg and 7 deg for the northern and southern pockmarks, respectively. The center ADCPs were oriented at a significant angle of about 24 deg and 17 deg within the northern and southern pockmarks, respectively. However, these tilt angles were internally accounted for within the RDI sensors when resolving the orthogonal velocity components and were consistent with the bathymetric slopes at the estimated location of the ADCPs. Because each ping, 0.35 s was adjusted for orientation, there are no adverse effects in the estimated current structure as a result of the non-leveled position of the ADCPs. The same is true for the single-point Aquadopp current meter.
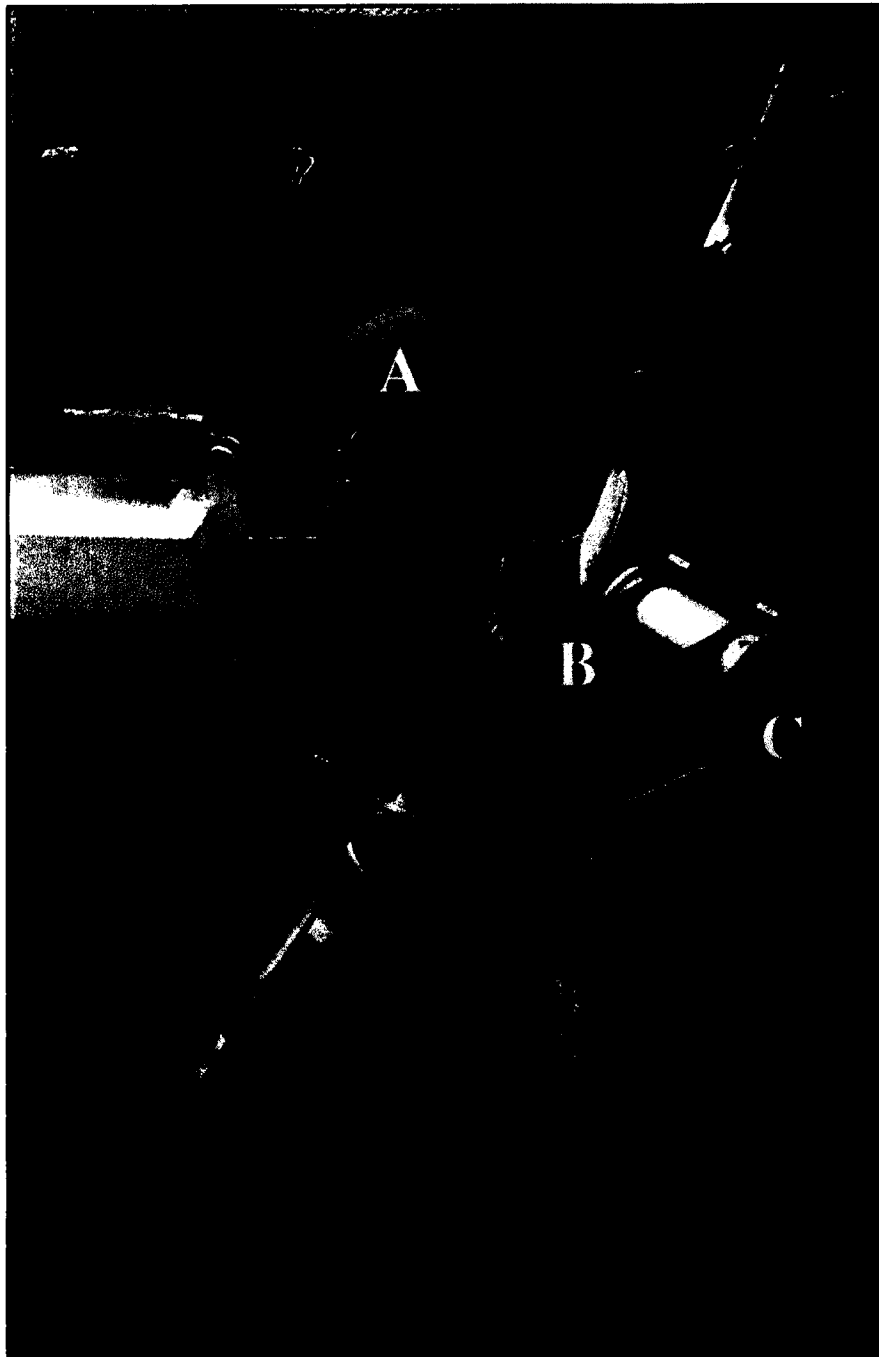
Figure 2-3. Image of current meter mount deployed in the center of each pockmark. The various parts labeled by letters are the (A) acoustic release, (B) RDI Workhorse 300 kHz ADCP and (C) Nortek Aquadopp acoustic current meter.

The estimated ADCP locations and approximate beam angles based on observed tilt angles are shown in Figure 2-4 along a north-south cross-sectional view of the bathymetry collected over each pockmark. These bathymetric profiles are relative to mean sea level and indicate the nearly symmetrical shape of both pockmarks, yet more elongated morphology of the southern pockmark (length-to-width ~ 2.2) than the northern pockmark (width-to-length ~ 1.2). The rim pockmark ADCPs, deployed on nearly level ground, have all four acoustic beams that reach the sea surface at the same bin elevation, and thus can accurately observe current structure within a short distance of the surface. The ADCPs deployed at the center of each pockmark, however, were positioned at a significant angle that results in individual acoustic beams that extend to different elevations within the water column. Measurements obtained beyond the maximum elevation sampled by all beams were eliminated. This maximum elevation was around 4 m and 8 m below the surface over the northern and southern pockmark, respectively.

Northern Pockmark

Southern Pockmark
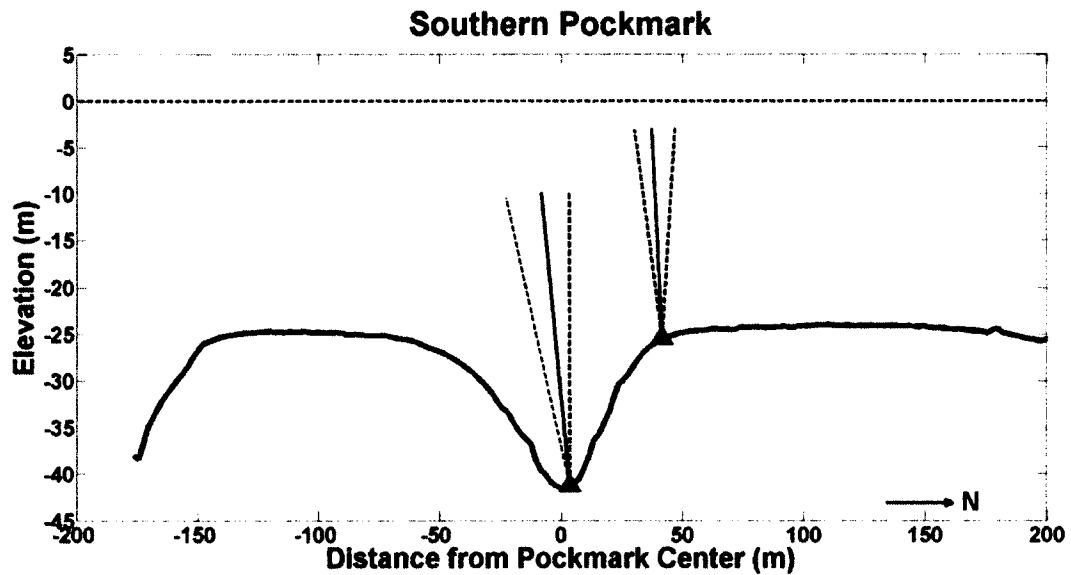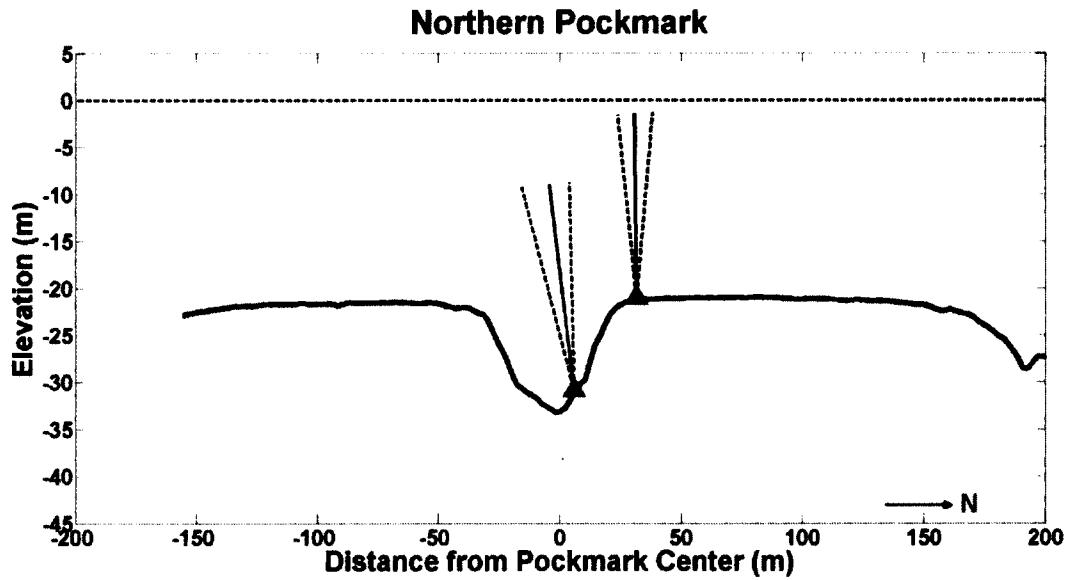
Figure 2-4. N-S cross-sectional view of bathymetry across each pockmark with the x-axis indicating the distance from the approximate pockmark center and the y-axis indicating elevation referenced to mean sea level. The approximate location of each current meter mount is marked by a gray triangle. The extension of the acoustic beams from the current meter mounts are marked by solid and dashed lines. Note, current data collected at ranges greater than the maximum distance reached by all acoustic beams were eliminated.

16

2.3.3 CTD Observations

CTD casts were obtained near the center of each pockmark at 2 *hr* intervals for a single tidal cycle to assess the time-varying structure of the water column over each pockmark. Data were acquired using a Seabird 19 CTD profiler and post-processed using the SeaBird data processing software. The density structure over both pockmarks was impacted by salinity and temperature variations with depth. Accuracy of the conductivity, used to derive salinity, and temperature sensors of the Seabird profiler were estimated to be within 0.001 *S/m* and 0.01°C, respectively based on manufacturers specification. Additionally, seawater temperature was measured over 5 *min* periods at the ADCP transducer locations in both RDI instruments and the Nortek Aquadopp. Temperature sensor accuracy of the Nortek Aquadopp and RDI ADCPs is 0.1°C and 0.4°C, respectively. These observations were calibrated *in situ* using the Seabird CTD observations.

In the following, a right-handed coordinate system is adopted with vertical datum at mean sea level and z coordinate positive upwards.

2.4 Results

2.4.1 Environmental Conditions and Depth-averaged Currents

Depth-averaged current data and wind conditions observed during the field experiment are displayed in Figure 2-5. Hourly averaged wind speed, direction, and gusts are indicated for both wind stations in Belfast and Searsport. Observed winds showed oscillations related to the diurnal sea breeze with speeds increasing in the late afternoon. Wind directions were determined by weak frontal systems that caused abrupt 180 *deg* changes every couple of days. Winds rotated from northeast to southwest during the northern pockmark deployment period and oscillated between northeast and southwest during the southern pockmark sampling period.

Current magnitude and direction data are depth-averaged over 3 layers including the surface layer from the surface to the approximate average depth of the thermocline, about 8 *m*, the mid-water layer from 8 *m* to the depth of the rim, and the deep layer from the rim depth to the bottom of the pockmark (Figure 2-5). Current direction data represent the direction that the current is flowing. Tidally-oscillating surface flow is modified by wind-driven currents and ranges in magnitude from 0 to 0.25 *m/s*, but is typically in the range 0.05 to 0.10 *m/s*.

The mid-water column currents ($8\ m < z <$ rim depth) are more strongly tidally dominated, particularly in the southern pockmark where current oscillations closely follow tidal phases. Mid-water column currents over the northern pockmark are more variable and influenced by wind-driven stress at the surface as well as converging tidal currents around Islesboro Island. Current magnitudes range from 0 to 0.20 *m/s* in this layer, and are typically stronger than the surface or deep currents indicating a sub-surface maximum in the current vertical structure due to the high-velocity tidal flow. Similar current observations at the rim and center of each pockmark suggest a nearly uniform horizontal variation in the flow from the rim to the center at mid depths.

The currents in the deep layer ($z <$ rim depth) are much weaker, ranging from 0 to 0.05 *m/s*, and do not always show strong tidal oscillations. Rotational structure in the deep layer is complex with currents rotating both clockwise and counter-clockwise over depth and varying in structure through time.

NORTHERN POCKMARK   SOUTHERN POCKMARK
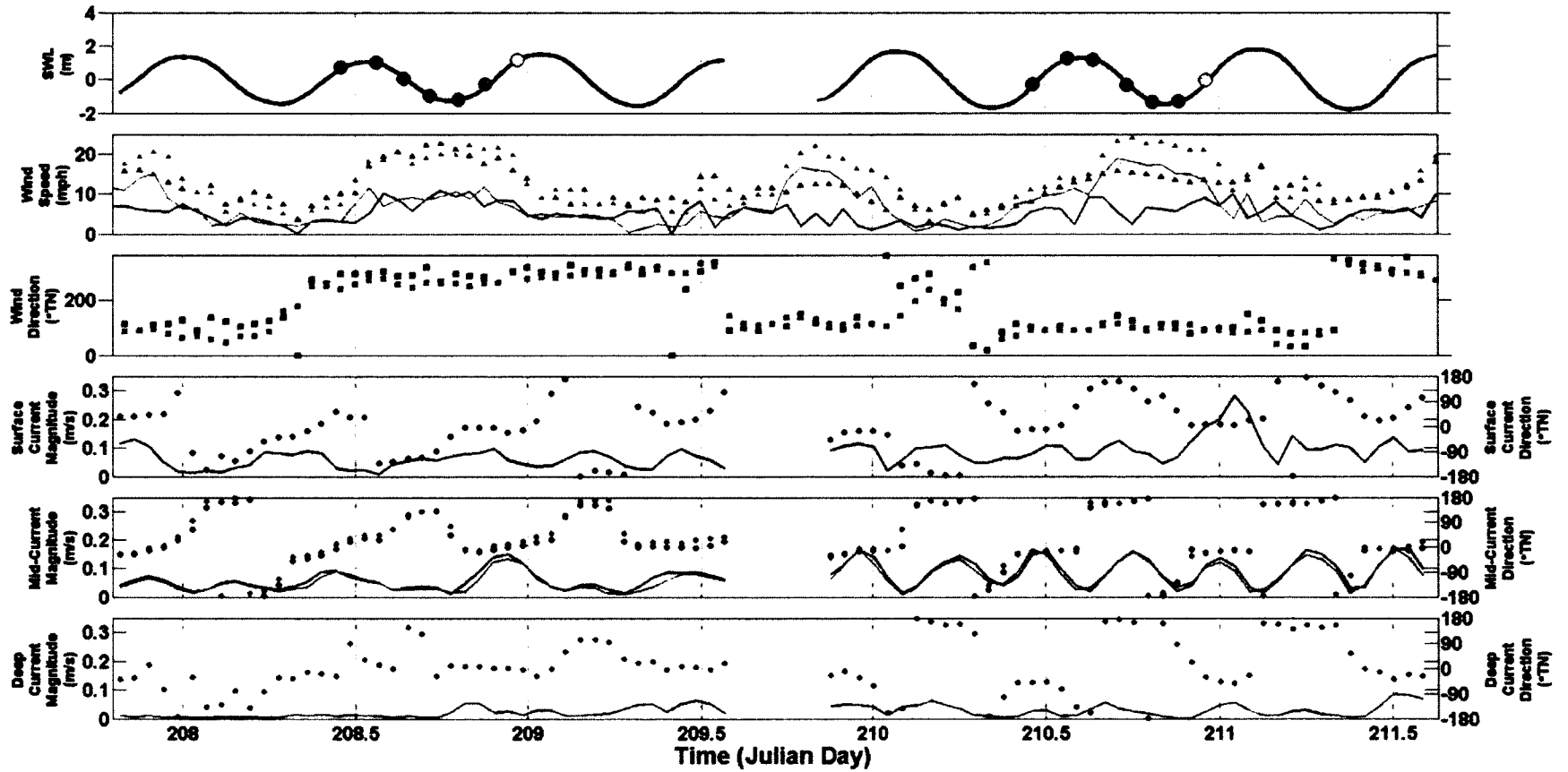
Time (Julian Day)

Figure 2-5 (Previous Page). Tide, wind and depth-averaged currents during the northern and southern pockmark sampling periods with time (Julian Days) on the x-axis. Upper panel shows mean sea surface elevation from bottom pressure data and the times (circles) of the CTD casts. Wind speed and direction obtained from meteorological stations near Belfast (light gray) and Searsport (dark gray) are shown in the next 2 panels. Triangles indicate hourly wind gusts. Lower 3 panels show hourly-averaged current magnitude directions depth-averaged over the surface, mid, and deep layers, respectively, delineated by the average depth of the thermocline (8 m) and depth of the pockmark rim (21 and 24 m). Data displayed in blue were obtained from the current meter mount located along the rim of either pockmark and data displayed in teal were obtained from the current meter mount located at the center of either pockmark.

2.4.2 Salinity and Temperature Observations

Variation of salinity and temperature profiles show strong density structure over the northern and southern pockmarks. The time-varying salinity and temperature structure of the water column was observed from multiple CTD casts acquired over the center of each pockmark (Figure 2-6). Salinity profiles show a general increase in salinity with depth near the surface and constant salinity below about 10-13 m depth. Sharp excursions in the salinity profiles of about 0.5 psu occur around 5 m and 12 m depths below the surface. These salinity variations may represent an advected flow from a previous mixing event.

Temperature profiles show diurnal thermal heating and cooling effects throughout the day with a characteristic deepening of the thermocline around mid day. Uniform temperatures are observed to extend from a few meters above the rim to the bottom of the pockmark, suggesting a homogeneous, well-mixed deep layer throughout the depression. An increase in temperature is observed in the last two casts obtained over the northern pockmark and was also recorded by the bottom-mounted ADCP temperature sensors. The observed rise in temperature evolved uniformly across the profile and extended to the bottom of the pockmark.
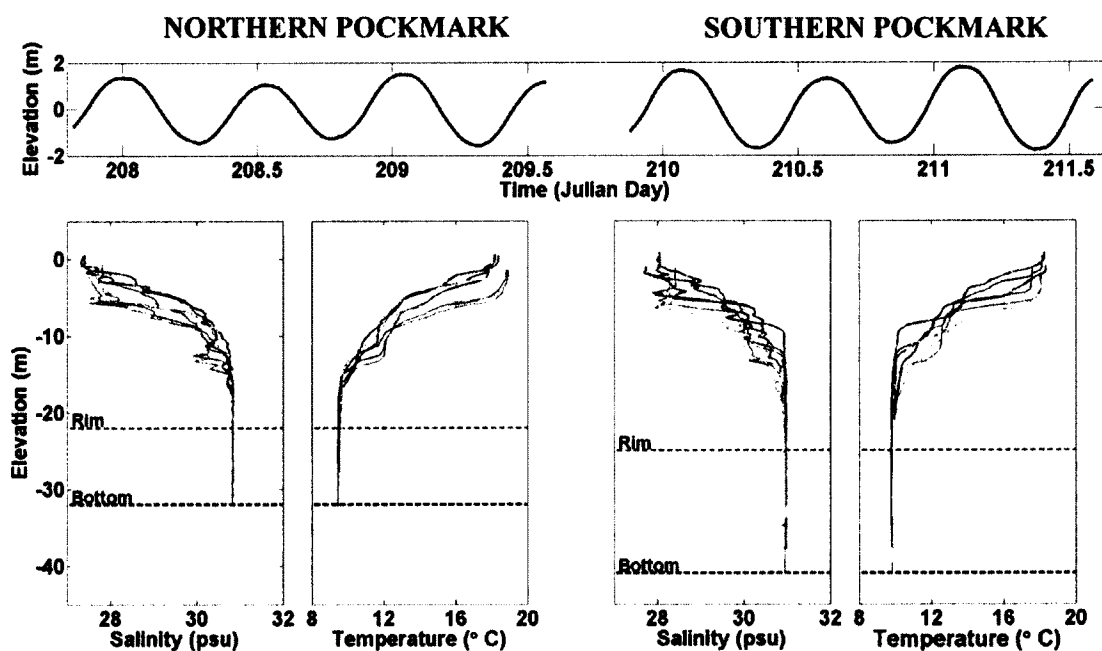
Figure 2-6. Salinity and temperature profiles acquired over the center of the northern (left panel) and southern pockmark (right panel). The upper panel shows tidal observations during the moored current meter sampling period where gray dots along the tidal wave indicate the time at which the individual CTD casts were acquired. Horizontally dashed gray and black lines denote the depth of the rim and bottom of each pockmark, respectively.

The time evolution of the near-bottom temperature recorded by the rim and center ADCPs is displayed in Figure 2-7. A $0.3°C$ rise in temperature beginning at Julian Day 208.8 occurs over an approximately 6 *hr* time period. The apparent time lag in temperature recorded at the rim and center of each pockmark is related to the relative location of the temperature sensor within the two ADCPs. At the rim, the ADCP temperature sensor is located internally, whereas at the center, the ADCP temperature sensor is located externally and therefore more quickly responds to changes in temperature. Depth-averaged vertical velocities below the rim from the center mounted ADCP show up and down-welling events, with magnitude of about 0.1- 0.15 *m/s* coincident with the rise in temperature and suggest a strong vertical mixing event extended from the center of the pockmark to above the rim (Figure 2-7). The initial rise in temperature occurred coincident to relatively strong upward-directed vertical velocities below the rim and is followed by a similarly strong down-welling event that decreases in magnitude as the temperature stabilizes. At the southern pockmark, a similar gradual rise in temperature was measured at both the rim and center ADCP locations, and was associated with a weak, net downward velocity over the duration of the deployment period.

Northern Pockmark Deployment   **Southern Pockmark Deployment**
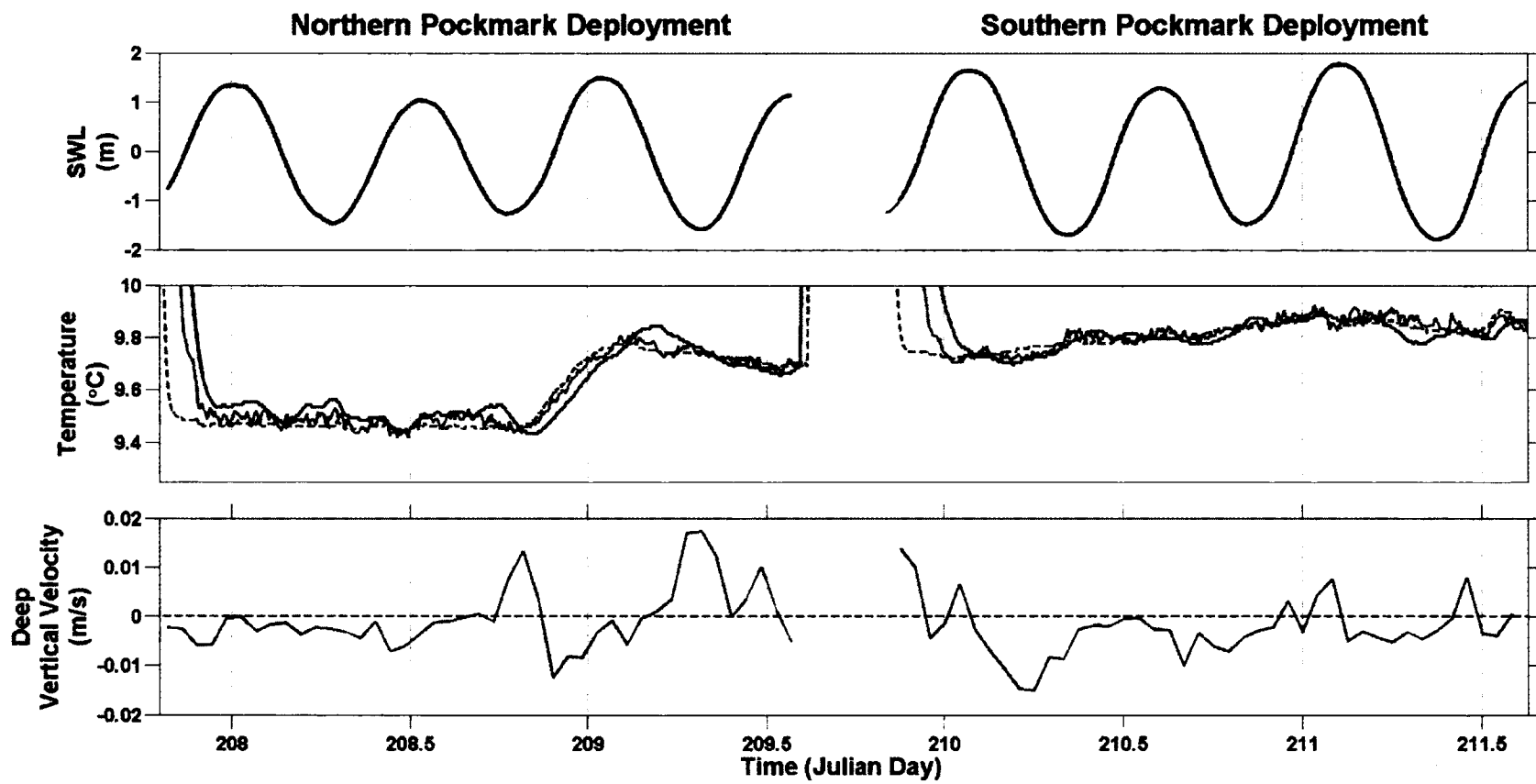
Figure 2-7 (Previous Page). Tidal, temperature and depth-averaged vertical velocity observations as a function of time (Julian Day) on the x-axis. The upper panel shows sea surface elevation from bottom pressure data. The middle panel shows temperature data acquired from temperature sensors along the rim (blue) and center (teal) current meter mounts. The solid and dashed lines denote temperature data acquired by the RDI Workhorse ADCPs and Aquadopp current meter, respectively. The lower panel shows depth-averaged vertical velocities below the rim averaged over 1 *hr* intervals. The dashed red line denotes 0 *m/s*.

2.4.3 Mean Current Vertical Structure

The temporal evolution of the vertical structure of hourly-averaged vertical velocities measured from the center ADCP in both the northern and southern pockmarks is shown in Figure 2-8. Typical vertical velocities are in the range of ± 0.02 *m/s* and show strong vertical structure and temporal variability. The data indicate strong up and downwelling events over the center of each pockmark that extend from above the rim and well into the pockmark.

Three distinct up-welling events were observed during the northern pockmark sampling period, each occurring around slack low tide and into the rising flood. The first event occurs coincidently with the observed temperature rise recorded by the CTD casts and fixed temperature sensors, discussed above, and is followed by a relatively strong downwelling period. Vertical velocities over the southern pockmark indicate a more tidally modulated pattern of up and downwelling periods that extend over a greater portion of the water column. Upward-directed vertical velocities typically occur during flooding tides and downwelling currents during ebbing tide.

Figures 2-9 and 2-10 show the observed spatial and temporal variation in current magnitude and direction from both the rim and center ADCPs at the northern and southern pockmarks, respectively. Greater variability in vertical structure was observed over the northern pockmark where horizontal current velocities show a less tidally-driven component.
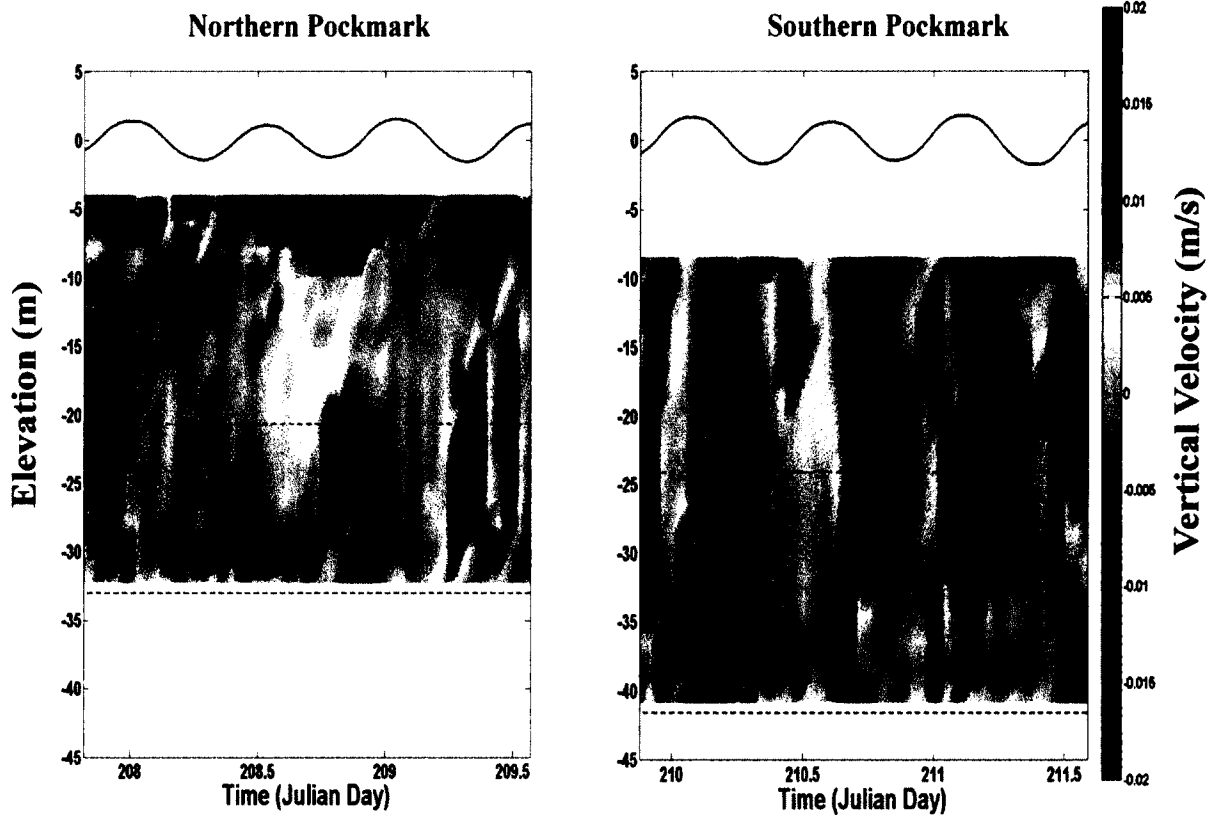
Figure 2-8. Hourly-averaged vertical velocity data over the northern (left panel) and southern pockmark (right panel) with the x-axis indicating time in Julian days and the y-axis denoting elevation relative to mean sea level. Vertical velocities range from -0.02 – 0.02 m/s where positive values indicate upward-directed flow and negative values denote downward-directed flow. The rim and bottom of each pockmark are marked by orange and black dashed lines, respectively.

28

Overall current velocities decrease in magnitude with depth and show increased complexity in rotational structure below the rim. Surface currents are strongly influenced by transient changes in wind speed and show substantial spatial variability in rotational structure over the northern pockmark. Upper water column flow on Julian Day 208.8-209.0 is offset approximately 130 *deg* between the rim and the center of the northern pockmark. This spatial offset may be a result of increased wind speed or converging tidal flows influencing the vertical current structure. High-velocity mid-water column currents show a strong tidal dependence and a tidally-modulated sub-surface maximum over both pockmarks. This sub-surface maximum oscillates between 5 to 15 *m* depths and surface and mid-depth currents often extend down into the pockmarks, specifically at the southern location.

Low-velocity flow below the rim does not exceed 0.10 m/s and shows significant spatial and temporal variability in rotational structure. Current direction below the rim rotates both clockwise and counter-clockwise with depth and often exceeds 90 *deg* of rotation from the rim to the bottom of the pockmark. A counter-clockwise directional pattern is more consistently observed over the southern pockmark, whereas the directional structure over the northern pockmark is more variable. Flooding tidal conditions typically show a near-northerly flowing surface current that rotates 50- 90 *deg* with depth. During ebbing tidal conditions, directional changes with depth are greater and occur more abruptly, typically on the order of 180 *deg* around 10 *m* above the seafloor.
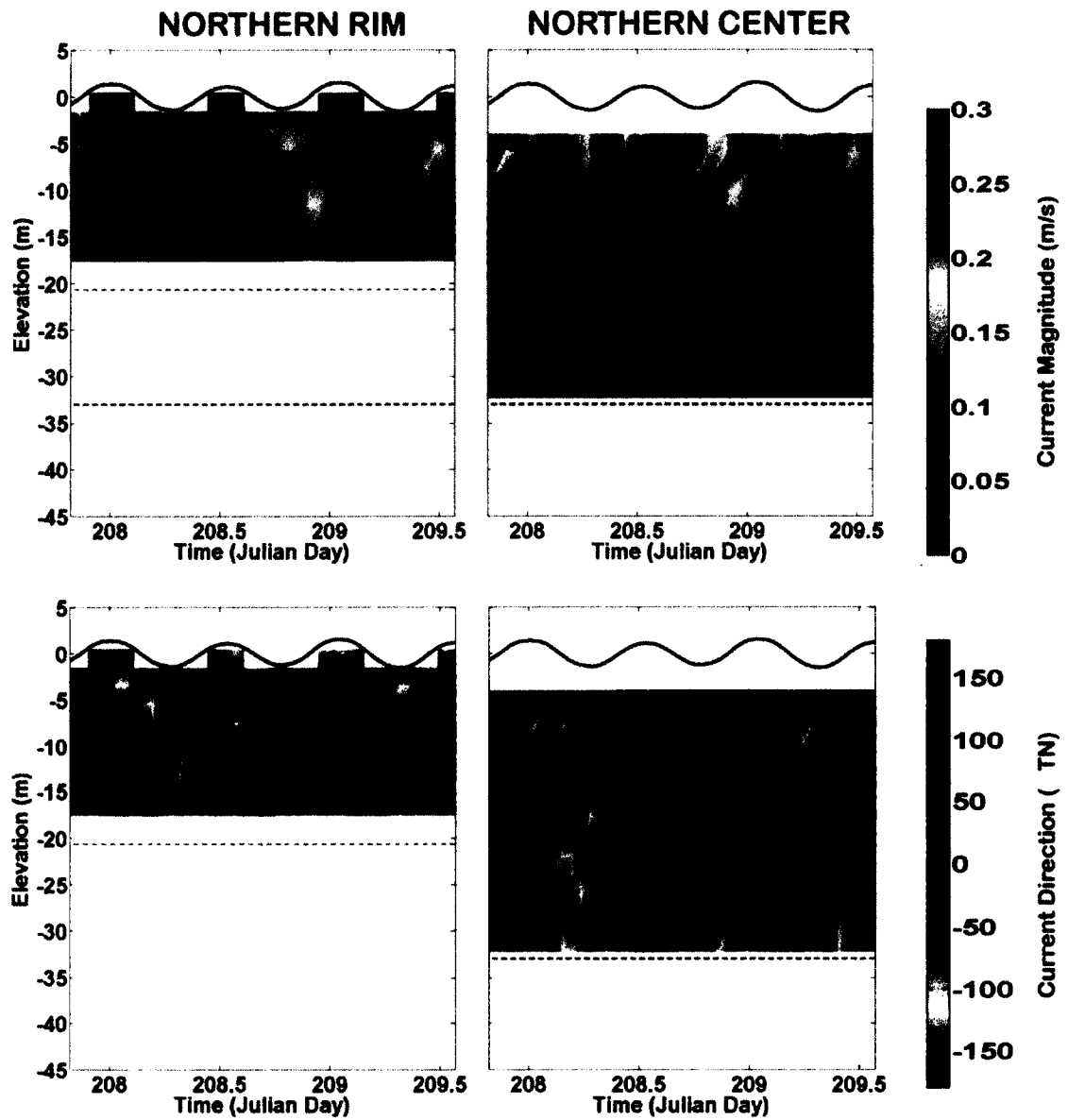
Figure 2-9. Hourly-averaged current magnitude (upper panel) and direction (lower panel) data acquried over the northern pockmark at the rim (left pannel) and center (right pannel) current meter mounts. The x-axis denotes time (Julian Day) and the y-axis shows elevation relative to mean sea level. Rim and bottom depths are marked by orange and black dashed lines, respectively.
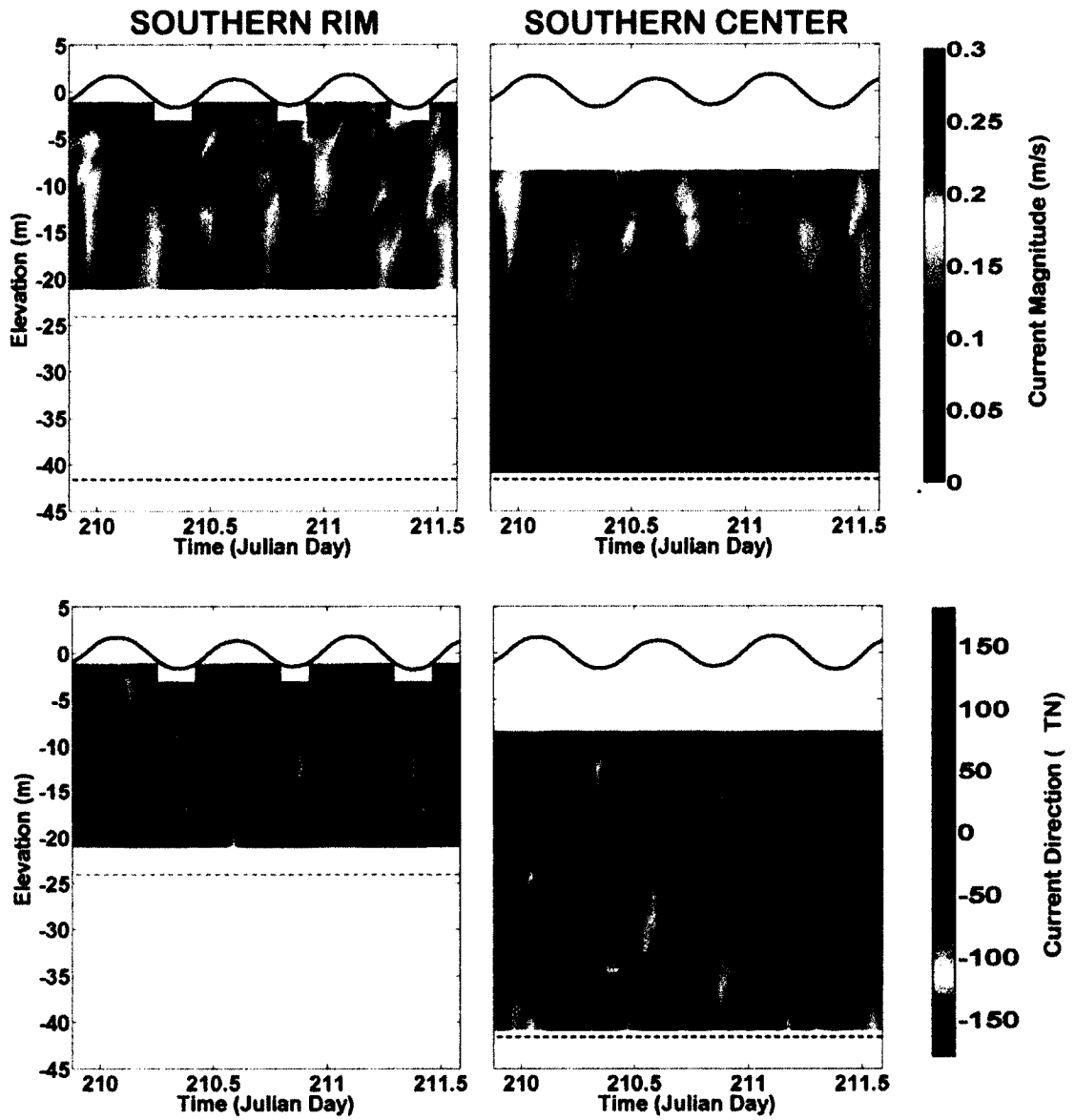
Figure 2-10. Hourly-averaged current magnitude (upper panel) and direction (lower panel) data acquried over the southern pockmark at the rim (left pannel) and center (right pannel) current meter mounts with the same layout as Figure 2-9.

2.5 Discussion

2.5.1 Mixing

Evidence of mixing and overturning over the sampled pockmarks comes from observations of uniform temperature and salinity structure below 15 m, a nearly simultaneous rise in temperature recorded at the rim and center of the northern pockmark, and strong vertical velocity events extending from above the rim and down into the pockmark. CTD observations reveal uniform temperature and salinity properties below 15 m which is indicative of a well-mixed water column and the interaction of flow above and below the rim (Figure 2-6). The absence of vertical temperature gradients over this depth allows for small changes in mixing to strongly affect the vertical structure of the water column. Therefore slight turbulent perturbations below 12 m can easily and rapidly mix this layer well down into the pockmark.

A nearly-simultaneous $0.3°C$ temperature rise was recorded by temperature sensors along the rim and center current meter mounts of the northern pockmark and occurred coincidently with a strong upwelling event followed by a downwelling event below the rim (Figure 2-7). This mixing event is similar in character to observations reported by Manley, *et al.* (2004) of overturning within a pockmark in Burlington Bay, Lake Champlain, Vermont. They observed increased wind stress at the surface that resulted in rapid cooling of the entire water column due to the replacement of warm, surface water by cold, deep water. This decrease in temperature was associated with strong negative vertical velocities that circulated water throughout the pockmark to create a homogeneous profile. These observations of temperature changes above and below the

32

rim of sampled pockmarks occurring concurrently with strong vertical velocity events indicate active mixing and overturning within these depressions.

Further evidence for mixing within pockmarks is provided by observations of strong upwelling and downwelling events that extended from above the rim down into the pockmark (Figure 2-8). Highest magnitude vertical velocities (order 0.15 *m/s*) typically occur slightly below the rim of the pockmark, presumably due to inner-pockmark circulation patterns. These vertical velocity observations are similar to numerically modeled results of flow over a pockmark obtained by Hammer, *et al.* (2009). They observed highest vertical velocities within the modeled pockmark that decreased in magnitude towards the surface and were induced by the geometry of the depression. These strong vertical velocity observations within the sampled and previously modeled pockmarks suggest internal pockmark mixing is most likely enhanced by pockmark geometry.

2.5.2 Mean Current Vertical Structure

Current structure is subdivided into three distinct layers at upper, mid, and deep regions marked by the average depth of the thermocline and the depth of the rim (Figures 2-5, 2-9 and 2-10). Upper-water column currents were influenced by wind stress at the surface and fluctuate in magnitude and direction in response to transient changes in wind speed. Mid-water column currents were the most strongly tidally-dominated layer and show a sub-surface maximum that oscillates with the tide and extends over a large portion of the water column. Deep water-column structure was highly complex and varied both temporally and spatially over each pockmark. Ebbing tidal conditions

33

typically show complete flow reversal at 10 m above the bed, whereas flooding tidal conditions show a lesser degree of rotation from surface to depth, typically on the order of 50 – 90 deg. Current observations over the northern pockmark show greater vertical and temporal variability that may be influenced by the geometry of Belfast Bay and the convergence of currents around Islesboro Island.

Xue, *et al.* (2000) developed a three-dimensional circulation model of Penobscot Bay to examine local circulation and temperature patterns within the bay. The modeled trajectories of particles released south of Deer Island show both clockwise and counterclockwise circulation around Islesboro Island during summer 1998 conditions at surface (6-10 m) and mid-water (30-40 m) depths (Xue and Brooks, 2000). These observations suggest converging tidal currents around Islesboro Island may describe the circulation pattern within Belfast Bay as well as explain the more complex vertical structure observed over the northern pockmark. The more-northern location of the northern pockmark is subjected to converging tidal currents entering the bay from the east and west of Islesboro Island to create a complex flow pattern over the pockmark. Conversely, the proximity of the southern pockmark to the narrow channel to the west of Islesboro Island results in more unidirectional, tidally-driven current observations.

2.5.3 Form Drag

Individual horizontal velocity profiles over each pockmark were investigated to assess the influence of pockmark geometry on the local flow structure. Current velocities past large roughness elements are often retarded due to contributions from skin friction and form drag. Skin friction refers to the tangential stress at the boundary, whereas form

34

drag results from pressure differences across the object and is produced by flow separation and internal wave generation (McCabe, *et al.*, 2006). Chriss and Caldwell (1982) were among the first to describe observations of form drag within subaqueous horizontal velocity profiles. Their observations of multiple logarithmic regions with slopes that increased with distance from the bed suggest that turbulent stress farther from the bed was greater than it was closer to the bed and concluded that boundary layer flow was significantly influenced by form drag.

The influence of form drag on the local flow regime in Belfast Bay was investigated by examining the hourly-averaged horizontal velocity profiles obtained from the bottom-mounted current meter observations at the center of each pockmark (Figure 2-9). The nature of the vertical structure in horizontal flow can be examined by looking for periods of logarithmic current structure near the seabed. A fully turbulent boundary layer forms due to the development of turbulent eddies close to the seafloor as a result of the overriding flow experiencing friction with the bed. A turbulent boundary layer flow can be characterized by a logarithmic velocity profile extending from the seafloor, assuming a no slip condition at the bed (Tennekes and Lumley, 1972). This logarithmic velocity profile is modeled as a function of friction velocity (u_*) and height (z) above the bottom, with

$$U(z) = \frac{u_*}{k} ln\left(\frac{z}{z_o}\right) \tag{2.1}$$

where $U(z)$ is the velocity at height z above the bottom, $k = 0.41$ is the von Karman coefficient, and z_o is the roughness length scale that varies with grain size and bedform

characteristics. Logarithmic regions were identified in this study using a simple, semi-automated algorithm that compared the observed velocity profile to a linear modeled profile in logarithmic space. The skill, S, of the model fit was determined by

$$S = \left(\frac{\sum(U(z)_{model} - \overline{U(z)_{model}})^2 / N}{\sum(U(z) - \overline{U(z)})^2 / N} \right)$$

(2.2)

where $U(z)$ and $U(z)_{model}$ are the horizontal velocity profiles of the observed and modeled data, respectively, and N is the number of depth-averaged measurements within the profile. Modeled profiles comprised of three or more data points, with a positive slope, and with skill less than two standard deviations from the skill mean were defined as having a logarithmic region near the bed; all other profiles were characterized as non-logarithmic. For profiles with a logarithmic profile, a second model was applied to data further up in the water column beginning at the highest velocity observation of the first logarithmic layer. In this manner, a second log layer could be observed. The presence of a second logarithmic layer is indicative of form drag resulting from turbulent processes generated by roughness elements located upstream of the velocity measurements (Arya, 1975). Form drag was observed to be significant in the vicinity of the sampled pockmarks based on observations of dual logarithmic layers occurring within individual horizontal velocity profiles. The form drag component of the total boundary layer stress in this region of Belfast Bay most likely originated from turbulent processes occurring over nearby, upstream pockmarks.

Horizontal velocity profiles over the northern and southern pockmarks indicate periods of no observable logarithmic region, a single logarithmic region, and a dual

36

logarithmic region (Figure 2-11). A greater frequency of single logarithmic regions are observed within the hourly-averaged horizontal velocity profiles over the northern pockmark, yet a second logarithmic region is more regularly observed over the southern pockmark (Figure 2-12). The second logarithmic region consistently occurs during flooding tidal conditions over both pockmarks and may be related to the higher velocity tidal flows during this time.

Similar to observations obtained by Chris and Caldwell (1982), the vertical gradient of the upper logarithmic region over the sampled pockmarks is always greater than the lower logarithmic region and suggests that roughness-induced form drag significantly contributes to the total boundary stress over the sampled pockmarks. Extending over a large portion of the water column, these logarithmic regions suggest the presence of enhanced turbulence and active mixing in the vicinity of pockmarks. Furthermore, observations of strong vertical velocity events and uniform temperature observations extending from above the rim down into the pockmark in conjunction with multiple logarithmic regions within the horizontal velocity profiles provide evidence for mixing and recirculation over both pockmarks.
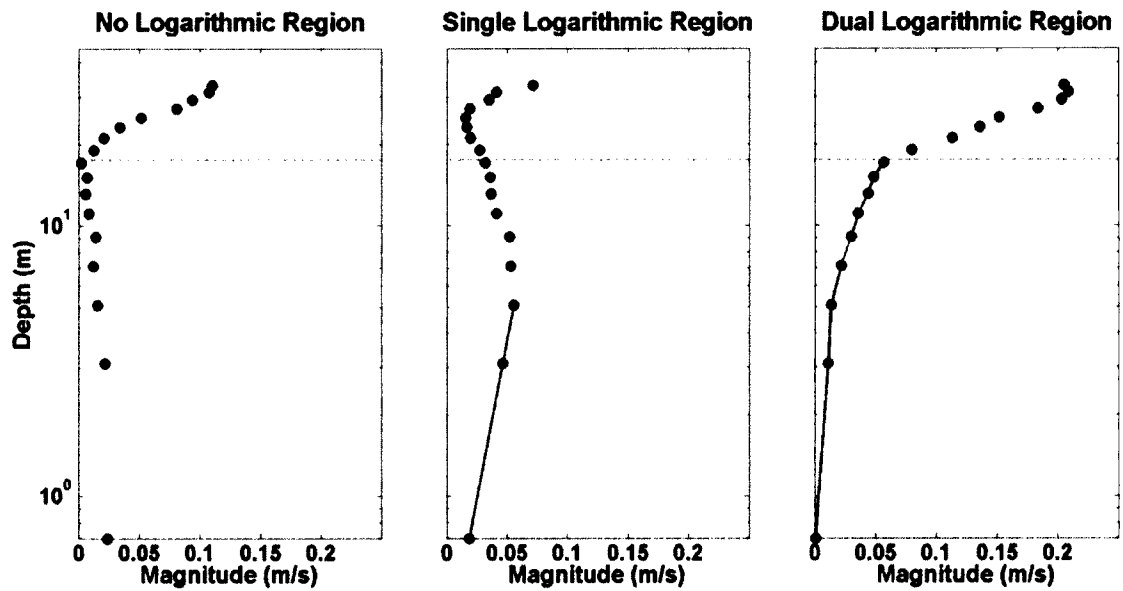
Figure 2-11. Example hourly-averaged horizontal velocity profiles obtained over the southern pockmark and displayed in semi-logarithmic space. The y-axis denotes elevation relative to mean sea level on a logarithmic scale and the x-axis shows current magnitude ranging from 0 to 0.25 m/s. Profiles show observations of no logarithmic region (left panel), a single logarithmic region (middle panel), and a dual logarithmic region (right panel).
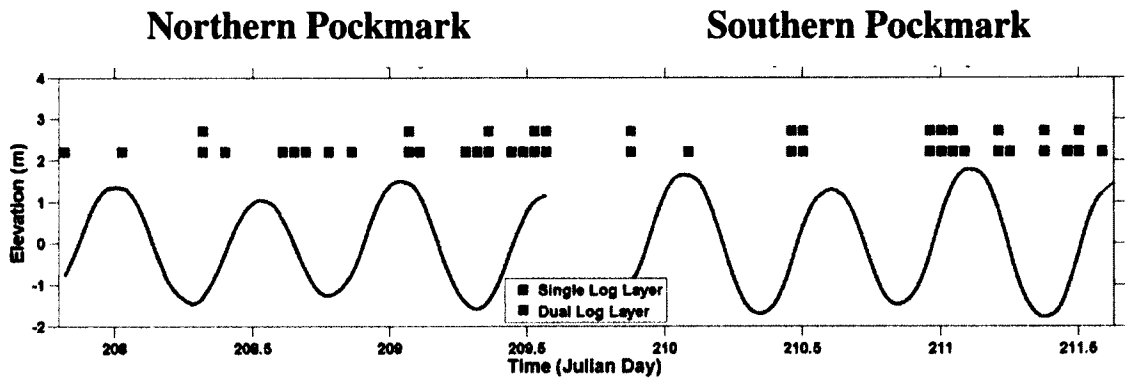
Figure 2-12. Observations of single and dual logarithmic regions over the center of the northern and southern pockmark. Profiles observed to have a single logarithmic region are denoted by a gray square and profiles with dual logarithmic regions are denoted by a black square. Note, a second logarithmic region was only defined during time periods over which the semi-automated algorithm defined a single logarithmic region.

2.6 Conclusions

Temperature, salinity, and current observations acquired over two pockmarks in Belfast Bay, Maine indicate a well-mixed vertical structure over a large portion of the water column and suggest form drag significantly influences boundary layer flow over pockmarks. Mean current vertical structure shows three distinct regions that are separated by the thermocline and rim depth. Variations in surface current magnitude and direction are primarily controlled by temporary changes in wind speed, whereas mid-water column flow is mainly tidally-modulated. A sub-surface maximum occurs around 5 to 15 m depth below the surface and fluctuates with the tide. Low-velocity currents below the rim show complex rotational changes with depth that are typically greater and in excess of 90 deg during the ebbing tide.

Temperature and salinity profiles in conjunction with vertical velocity observations over each pockmark suggest mixing and overturning are actively occurring over these depressions. Uniform temperature and salinity observations with depth are indicative of a well-mixed water column and are observed over each pockmark from 12 *m* depths to the bed. Furthermore, observations of a nearly simultaneous temperature rise recorded at the rim and center of the northern pockmark occurring with strong vertical velocities below the rim suggest active overturning of the water column. Observations of vertical velocity events extending from above the rim to down into the pockmark indicate active exchange of fluid within the pockmark.

The influence of form drag in the vicinity of the sampled pockmarks was investigated by examining hourly-averaged velocity profiles. Many velocity profiles showed multiple logarithmic regions which suggests form drag significantly influences the local flow regime. These observations of mixing and enhanced turbulence over the sampled pockmarks are consistent with field observations and modeled results of flow over pockmarks (Manley, *et al.*, 2004; Hammer, *et al.*, 2009; Brothers, *et al.*, 2011b).

Future studies should include long-term monitoring of the temperature and current patterns over multiple pockmarks to assess the influence of storm events on the vertical structure above pockmarks and better constrain circulation patterns within these depressions.

CHAPTER 3

OBSERVATIONS OF POCKMARK FLOW STRUCTURE IN BELFAST BAY, MAINE, PART 2: RECIRCULATION AND CAVITY FLOW

3.1 Abstract

Pockmark flow circulation patterns are investigated through current measurements along the rim and center of two pockmarks in Belfast Bay, Maine. Observed time-varying current profiles have a complex vertical and directional structure that rotates significantly with depth and is strongly dependent on the phase of the tide. Observations of the vertical profiles of horizontal velocities in relation to relative geometric parameters of the pockmark are consistent with circulation patterns described qualitatively by cavity flow models (Ashcroft and Zhang, 2005). The time-mean behavior of the shear layer is typically used to characterize cavity flow and was estimated using vorticity thickness to quantify the growth rate of the shear layer horizontally across the pockmark. Estimated positive vorticity thickness growth rates are qualitatively consistent with cavity flow predictions, but occur at largely different rates between the two pockmarks. Previously modeled flow patterns over pockmarks of similar geometry to those examined herein (Brothers, *et al.*, 2011b), are also conceptually consistent with cavity flow circulation. Therefore, Belfast Bay pockmarks of similar geometry to those

sampled in this study may also be characterized by circulation patterns predicted by open cavity flow.

3.2 Introduction

Pockmarks are crater-like depressions in the seafloor that are globally distributed and ubiquitous in nearshore environments (*e.g.*, Kelley, *et al.*, 1994). These depressions are believed to form from fluid and gas escape from underlying, unconsolidated sediment and range in size from a few meters to several kilometers in diameter (Hovland and Judd, 1988). The interaction of currents with seafloor depressions is poorly understood, but is of primary importance to circulation, mixing, and sediment transport within pockmarks. Current observations in the vicinity of pockmarks will improve ecological models that estimate faunal and nutrient dispersion patterns around pockmarks as well as better constrain sedimentation and erosion rate estimations within and around these prominent seafloor features.

Three previous studies have investigated current circulation within pockmarks. Manley, *et al.* (2004) conducted a long-term field study over a nearly circular pockmark with length-to-depth ratio (L/D) of approximately 10 in Burlington Bay, Vermont. Observations of strong, upward-directed vertical velocity events and flow recirculation within the pockmark are suggested to be consistent with back-eddy formation or the development of a cyclostrophic flow within the pockmark. Three-dimensional numerical modeling completed by Hammer, *et al.* (2009) examined current flow over a pockmark (L/D ~5.7) with similar dimensions to those found naturally in the Inner Oslofjord, Norway pockmark field. Modeled results showed contour-following currents with strong

upward-directed velocities in the center and along the downstream edge of the pockmark that conceptually agreed with the cyclostrophic flow model proposed by Manley, *et al.* (2004). Brothers, *et al.* (2011b) numerically modeled incompressible flow over a simplified pockmark in two and three dimensions. Their results show both contour-following and recirculating flow patterns within the pockmark as the relative length-to-depth ratio of the pockmark is altered and indicate that pockmark flow circulation is strongly influenced by the geometry of the depression.

In Chapter 2 of this thesis, we described field observations obtained in two pockmarks in Belfast Bay, Maine. These observations indicate active mixing and overturning throughout the pockmarks and the influence of roughness-induced form drag on the overall flow structure. This study investigates the relationship between pockmark geometry and internal circulation patterns using the same field observations obtained along the rim and center of the two sampled pockmarks (Figure 3-1).

Belfast Bay is located in the northwestern Gulf of Maine and is characterized by an extensive pockmark field in a shallow, estuarine environment with tidally-driven currents. Greater complexity in flow structure is observed over the northern pockmark due to converging tidal currents around Islesboro Island (Xue, *et al.*, 2000). The closer proximity of the southern pockmark to the narrow channel to the west of Islesboro Island results in more tidally-driven, unidirectional flow over the pockmark. This paper shows that a conceptual open cavity flow model (Ashcroft and Zhang, 2005) qualitatively predicts recirculation patterns within the two sampled pockmarks in Belfast Bay.
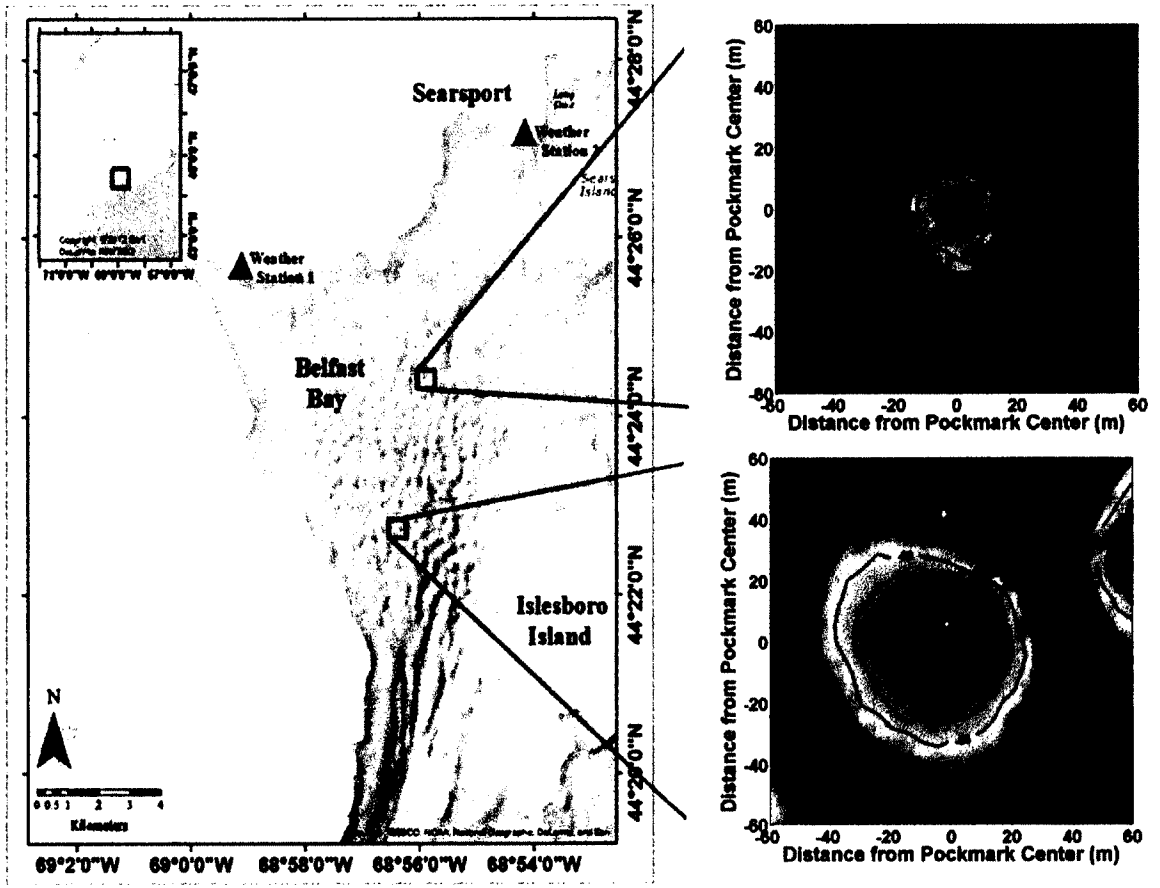
Figure 3-1. Overview map of Belfast Bay, Maine (left panel). Weather stations are denoted by gray triangles. The approximate locations of the northern and southern pockmarks are outlined by gray boxes. Bathymetric maps of the northern and southern pockmarks are shown in the upper right panel and lower right panel, respectively. The black/white circles and range bars denote the approximate location of the center and rim current meter mounts and their associated uncertainty.

3.3 Methods

Bathymetric and current measurements were obtained in July 2011 along the rim and center of two pockmarks in Belfast Bay (Figure 3-1). The field setting and observational methods are described in detail in Chapter 2 of this thesis and are only summarized here.

High resolution bathymetry was measured with a shipboard single beam echo sounder and gridded to 2.5 m resolution to define the geometry of the pockmarks (Figure 3-1). The pockmarks are located in the northern and southern regions of Belfast Bay and differ in relative geometry. The nearly-circular, northern pockmark is about 45 m in diameter and located within 21 m water depth with a length-to-depth ratio of 3.7. The more elongated, southern pockmark is approximately 85 m in diameter along the major axis dimension with a length-to-depth ratio of 4.7 in 25 m water depth. Tidal phases were determined from observations at a NOAA Tide gauge in Portland, Maine, to the south, and corrected for tide phase lags from Portland to Belfast.

Current velocities were measured by the center and rim bottom-mounted ADCPs in 0.5 m successive bins. Mean current data are reported as hourly-averaged velocities with 2 m vertical bin resolution. ADCP velocity accuracy is greater than 0.0025 m/s in all three dimensions.

The location of bottom-mounted ADCPs deployed on the rim and in the center of each pockmark was determined within about +/- 3.5 m accuracy. The center ADCPs were positioned slightly north of the pockmark center along the northeastern sidewall at a tilt angle of about 18-25 deg. This slightly offset position of the center current meter mounts to the northeast of each pockmark center is a distinction that is important to the

interpretation of the circulation pattern and growth of the shear layer across the pockmark that is predicted qualitatively by open cavity flow.

Currents behavior described in Chapter 2 show strong vertical structure and were sub-divided into three sections, the surface, middle, and deep water column delimited by the average depth of the thermocline, about 8 m below the surface, and the depth of the rim. Surface tidal flows range from 0 to 0.25 m/s and are modified by local wind-driven currents. Upper water column flow over the northern pockmark is further influenced by converging tidal flows around Islesboro Island. Mid water column currents are typically stronger than the surface flow and show greater tidal-dependency. A sub-surface maximum is observed over each pockmark around 12 m depth and fluctuates with the tide. Directional structure above the rim is tidally-modulated but rotates with depth clockwise and counter-clockwise depending on modification by wind-driven currents. Low-velocity currents below the rim range from 0 – 0.05 m/s and show a tidally-varying rotational structure. The time-mean behavior of rotational structure below the rim is the focus of this paper.

3.4 Results

Figure 3-2 shows the observed temporal evolution of the horizontal current rotational behavior with depth over each pockmark. Over the northern pockmark, the rotational structure is generally tidally-varying but has high temporal variability with horizontal currents that rotate both clockwise and counter-clockwise with depth and exhibit additional complexity below 10 m. Currents typically show a greater degree of rotation during the ebbing tide where flows below the rim often rotate more than 90 deg

from near-surface flow. Significant rotation with depth is also observed during the flooding tide, but to a lesser degree, on the order of 50 - 90 *deg*. A similar, tidally-varying rotational pattern is observed over the southern pockmark, but with less vertical and temporal variability perhaps due to the higher-velocity currents in the narrower region of the bay. Directional changes from surface to depth over the southern pockmark typically rotate in a counter-clockwise direction on the order of 90 - 180 *deg* during the ebbing tide and 50 - 90 *deg* during the flooding tide. At slack tides reversal of flow near the bottom of each pockmark leads the surface flow, consistent with typical boundary layer behavior where weaker near-bottom flows have less inertia and respond more quickly to changes in the forcing (Kundu and Cohen, 2008).

NORTHERN POCKMARK
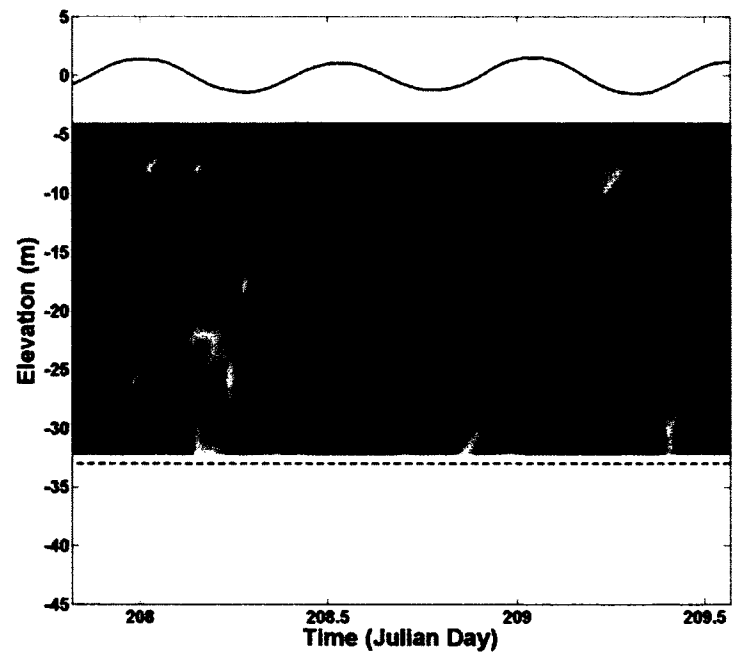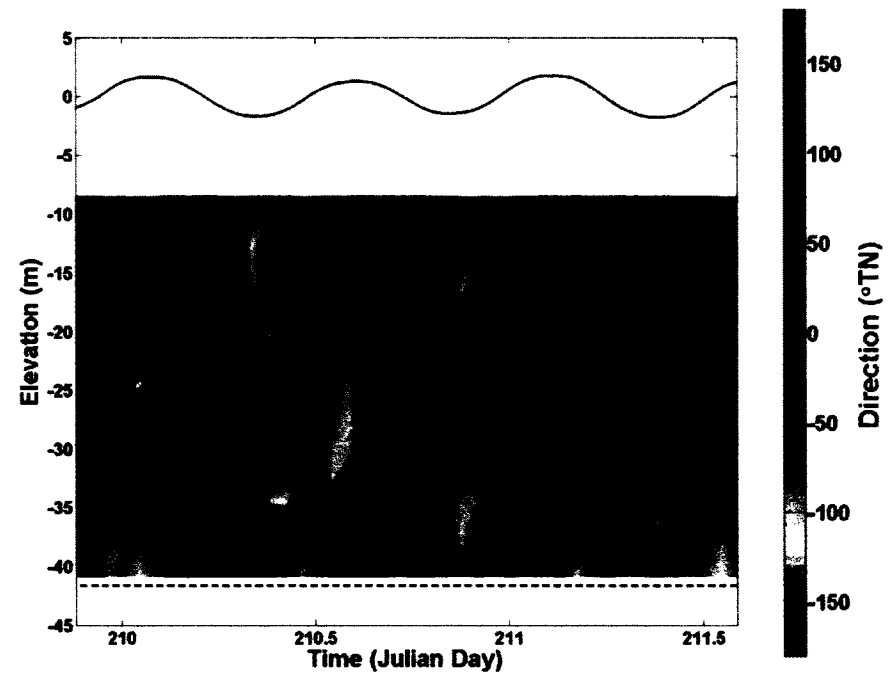
SOUTHERN POCKMARK

Figure 3-2 (Previous Page). Color-filled contour plots of current direction data obtained at the center of the northern and southern pockmark. Horizontal axis denotes time (Julian Day) and vertical axis shows depth relative to mean sea level. The dotted orange and black lines indicate the rim and bottom depth, respectively. Observed tidal oscillations are displayed over current observations as a solid black line.

Horizontal current direction profiles over 1 *hr* periods during maximum flooding and ebbing tidal phases are shown in Figure 3-3. As before, the overall vertical rotational structure shows a tidally-varying pattern over both pockmarks. Near-northerly directed flow above the rim is observed during the maximum flooding tides and rotates nearly 180 *deg* during maximum ebbing tidal conditions. Below the rim, significant and abrupt changes in rotation are observed that are typically greater during the ebbing tide. The sense of rotation from surface to depth varies over each pockmark. Over the northern pockmark, currents rotate both clockwise and counter-clockwise with depth, whereas over the southern pockmark, currents always rotate in a counter-clockwise direction during these maximum flow events. Flow over both pockmarks during maximum flooding tidal conditions is nearly northward at the surface and rotates approximately 50 - 100 *deg* with depth. As the tide ebbs, a greater degree of rotation is observed as currents rotate from 180 ± 50 *deg* near the surface to 0 ± 50 *deg* at depth. These significant directional changes below the rim typically occur at about 10 *m* above the seafloor, approximately mid-way between the rim and bottom of the pockmark. The observed rotation below the rim generally occurs more abruptly during the ebbing tide, especially over the southern pockmark. During the flooding tide, the rotation from surface to depth is less and occurs more gradually. These tidally-varying rotational patterns over both pockmarks resemble circulation patterns qualitatively predicted by open cavity flow and will be discussed later.

NORTHERN POCKMARK
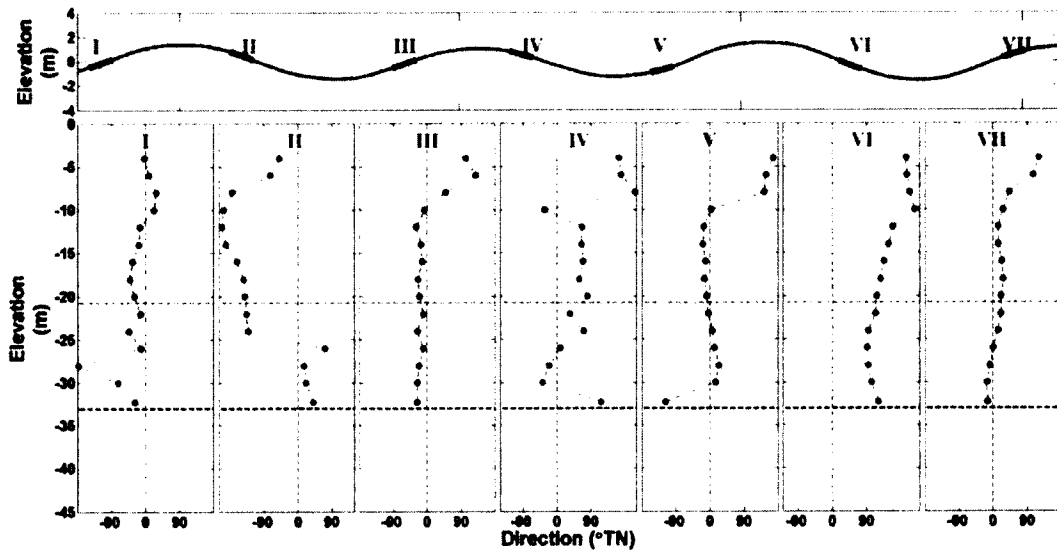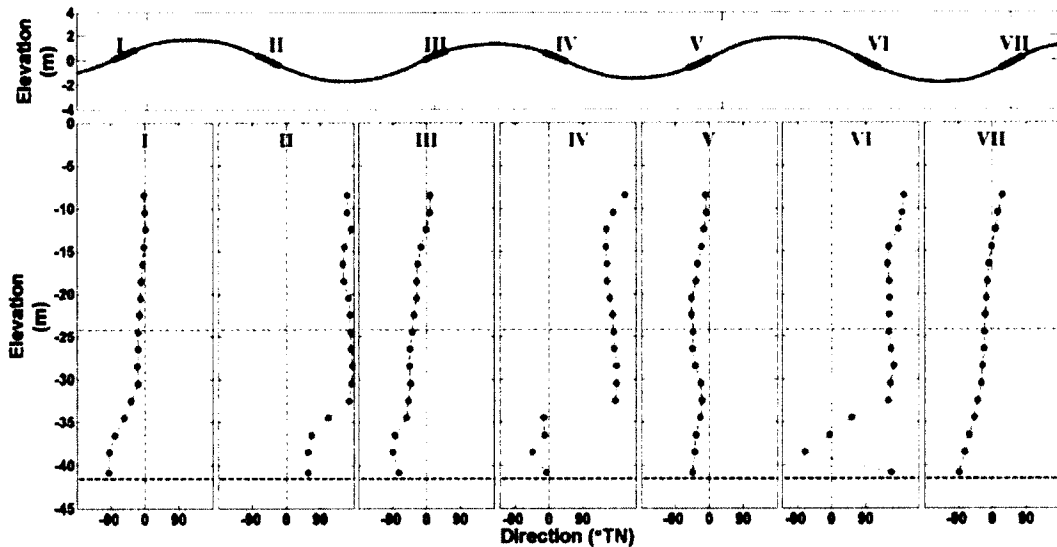
SOUTHERN POCKMARK

Figure 3-3. Hourly-averaged horizontal velocity direction profiles during maximum flooding (blue) and ebbing (red) tidal conditions from the center current meter mount in the northern (upper) and southern (lower) pockmark. Observed tidal oscillations are shown in the top panel. Highlighted bars along the tidal cycle with representative roman numerals each correspond to the hourly-averaged horizontal velocity direction profile shown in the lower panel. The horizontal axis of the lower panel denotes current direction where 0 *deg*, northerly flow, is marked by a vertically dashed gray line. The horizontally dashed orange and black lines in the lower panel denote the rim and bottom pockmark depth, respectively.

51

3.5 Discussion

The complexity of the horizontal velocity structure over the northern and southern pockmarks may be partly explained by the geographic location of the pockmarks within the bay (Figure 3-1). Relatively higher velocity tidal flow enters Belfast Bay through a narrow channel to the west of Islesboro Island. The proximity of the southern pockmark to this channel yields more strongly tidally-driven current observations than over the northern pockmark where increased complexity in horizontal current structure may be attributed to converging tidal currents around Islesboro Island (Xue and Brooks, 2000).

Vertically-varying rotational structure observed over the pockmarks show abrupt directional changes during the ebbing tide that are consistent with open cavity flow and the formation of a recirculation cell within the pockmark (Rockwell and Naudasher, 1978). Cavity flow patterns have been well-studied through multiple theoretical, empirical, and numerical investigations (*e.g.* Sarohia, 1977; Rockwell *et al.*, 1978; Ahuja and Mendoza, 1995). These studies have shown cavity flow circulation to be strongly influenced by numerous flow parameters including boundary layer thickness, freestream velocity, turbulence, and the geometry of the cavity. The time-mean behavior of the shear layer is typically used to characterize cavity flow and is described as the layer that forms as the overriding flow separates at the upstream rim of the cavity due to the geometry of the depression. The time-mean behavior of the shear layer is strongly dependent on the length-to-depth ratio of the cavity and subdivides cavity flow into two flow regimes: closed cavity flow and open cavity flow. Closed cavity flow predominantly occurs in shallow cavities ($L/D > 9$) and is characterized by the shear layer flowing into the cavity, reattaching along the base, and then separating again before the downstream wall.

Conversely, open cavity flow typically occurs in deeper cavities (L/D < 6) and is described by the shear layer passing over the cavity and reattaching along the trailing edge. Figure 3-4 shows a schematic that illustrates this point. The relatively small length-to-depth ratios of the northern (L/D ≈ 3.7) and southern (L/D ≈ 4.7) pockmarks suggest that circulation patterns within these depressions should resemble open cavity flow.
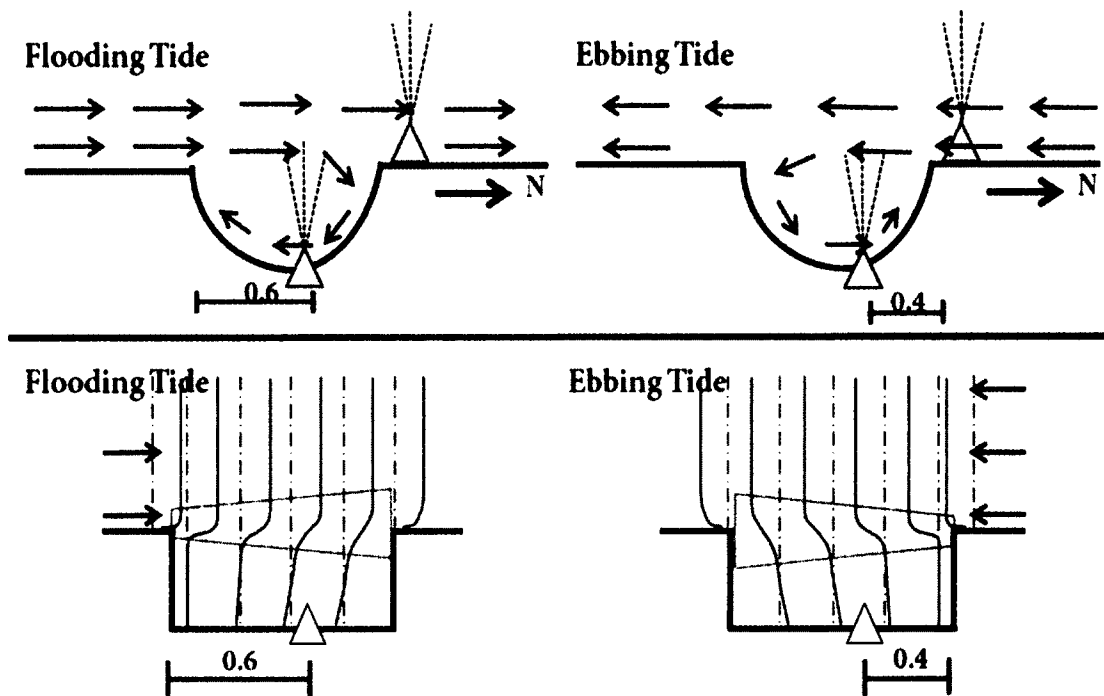
Figure 3-4. Schematic diagram of open cavity flow circulation and shear layer growth with distance downstream. The approximate location of the ADCPs within the pockmark is denoted by yellow triangles with relative distance downstream from the leading edge marked in red. The upper panel illustrates the predicted open cavity flow circulation patterns within the sampled pockmarks during the flooding and the ebbing tide. The lower-panel shows the temporally varying horizontal velocity direction profiles across a modeled cavity during flooding and ebbing tidal conditions and approximate shear layer growth with distance downstream (shaded orange region). The horizontal velocity direction profiles are centered on 0 *deg* which is marked by a dashed gray line. This figure was modified from Ashcroft and Zhang's (2005) Figure 3.

The time-mean development of the shear layer increases with distance downstream in open cavity flow and can be estimated using vorticity thickness (Ashcroft and Zhang, 2005). Vorticity thickness (δ_ω) is given by

$$\delta_\omega = \frac{U_2 - U_1}{\partial \langle U \rangle / \partial z|_{max_z}} \tag{3.1}$$

where U_1 is the velocity at the bed (assumed to be 0 m/s), U_2 is the freestream velocity and $\langle U \rangle$ is the time-mean velocity profile of the shear layer that varies with depth. Vorticity thickness was calculated at two length scales within each pockmark based on the relative location of the current meter mount with respect to the leading edge of the pockmark during the flooding ($0.6L$) and ebbing ($0.4L$) tide, where L is the diameter at the rim (Figure 3-4).

Figures 3-5 and 3-6 are sub-divided into three panels that show the temporally varying freestream velocity and maximum velocity gradient in the upper two panels used to calculate the vorticity thickness illustrated in the lower panel. The white regions in each panel denote slack tide, during which vorticity thickness was not estimated. The upper panel shows the temporal evolution of the horizontal current magnitudes acquired at the rim. The dashed gray lines outline the upper 8 m of the water column delimiting the depth range over which the maximum velocity was determined and denoted as the freestream velocity (U_2). The middle panel displays the vertical velocity gradient calculated from the hourly-averaged horizontal velocity data acquired by the center mounted current meter. The gray circle denotes the maximum gradient within the observed shear layer, which is outlined by the gray error bars. The lower panel shows the

temporal evolution of estimated vorticity thicknesses and is overlain by the observed tidal oscillations. Greater vorticity thicknesses were estimated during flooding tidal conditions and signify the growth of the shear layer with distance downstream. However, the rate at which the estimated vorticity thickness increased across the pockmark largely differed between the two pockmarks. Mean vorticity thickness estimations at the northern pockmark increased from 13.34 m during ebb tidal flow to 13.95 m during flood tidal flow at a spreading rate ($\partial \delta_\omega / \partial x$) of 0.061. Estimated mean shear layer growth rate over the southern pockmark was much greater (0.36) and nearly doubled from ebbing (8.62 m) to flooding (16.07 m) tidal conditions.

Spreading rate estimates across the sampled pockmarks are qualitatively compared to those obtained by Ashcroft and Zhang (2005) over a modeled deep cavity (L/D = 4) (Figure 3-7). Ashcroft and Zhang (2005) observed linear shear layer growth across the modeled cavity at a spreading rate of 0.14. The variability in spreading rates observed over the modeled deep cavity and the sampled pockmarks may be attributed to the geometric differences between these depressions. Modeled cavity geometry is defined by vertical sidewalls and a flat base whereas the Belfast pockmarks were conical in nature with an approximate 30 deg sidewall slope. The influence of non-vertical sidewalls as well as proximity and influence of flow over other regional cavities are unaccounted for in this model and may account for some of the differences in spreading rate estimates. Although large variability in spreading rates were observed over the sampled pockmarks, observations of flow reversal near the base of the pockmarks and downstream growth of the shear layer are consistent with open cavity flow and suggest cavity flow may describe the nature of pockmark flow circulation in the pockmarks in Belfast Bay.
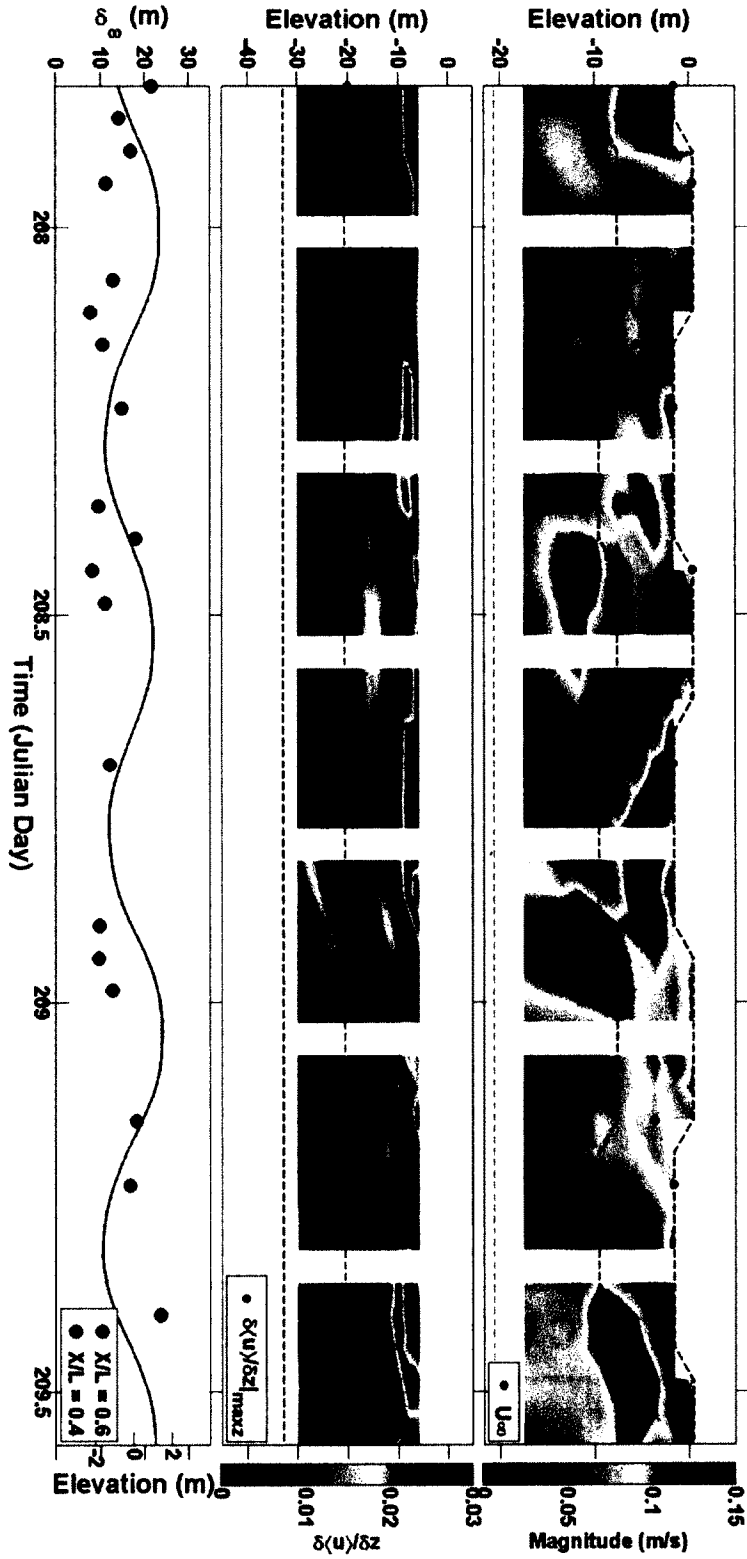
Figure 3-5 (Previous Page). Vorticity thickness estimations over the northern pockmark. Vorticity thickness was not estimated during slack tide so data during this time interval are not displayed. The horizontal axis denotes time in Julian Days and the horizontal dashed orange and black lines in the upper two panels denote the rim and bottom pockmark depth, respectively. The upper panel shows current magnitude data acquired at the rim. Dashed gray lines outline the upper 8 *m* of the water column from which a maximum velocity was chosen and denoted as the freestream velocity (gray dot). The middle panel denotes the vertical velocity gradient over the center of the pockmark. The maximum gradient in velocity within the shear layer is marked by a gray dot, where vertical gray error bars denote the depth range over which the shear layer was defined. The lower panel shows estimated vorticity thicknesses during the flooding (blue) and ebbing (red) tide and are overlain by tidal observations. Note vorticity thickness was only estimated when a shear layer was observed in the hourly-averaged velocity profile.
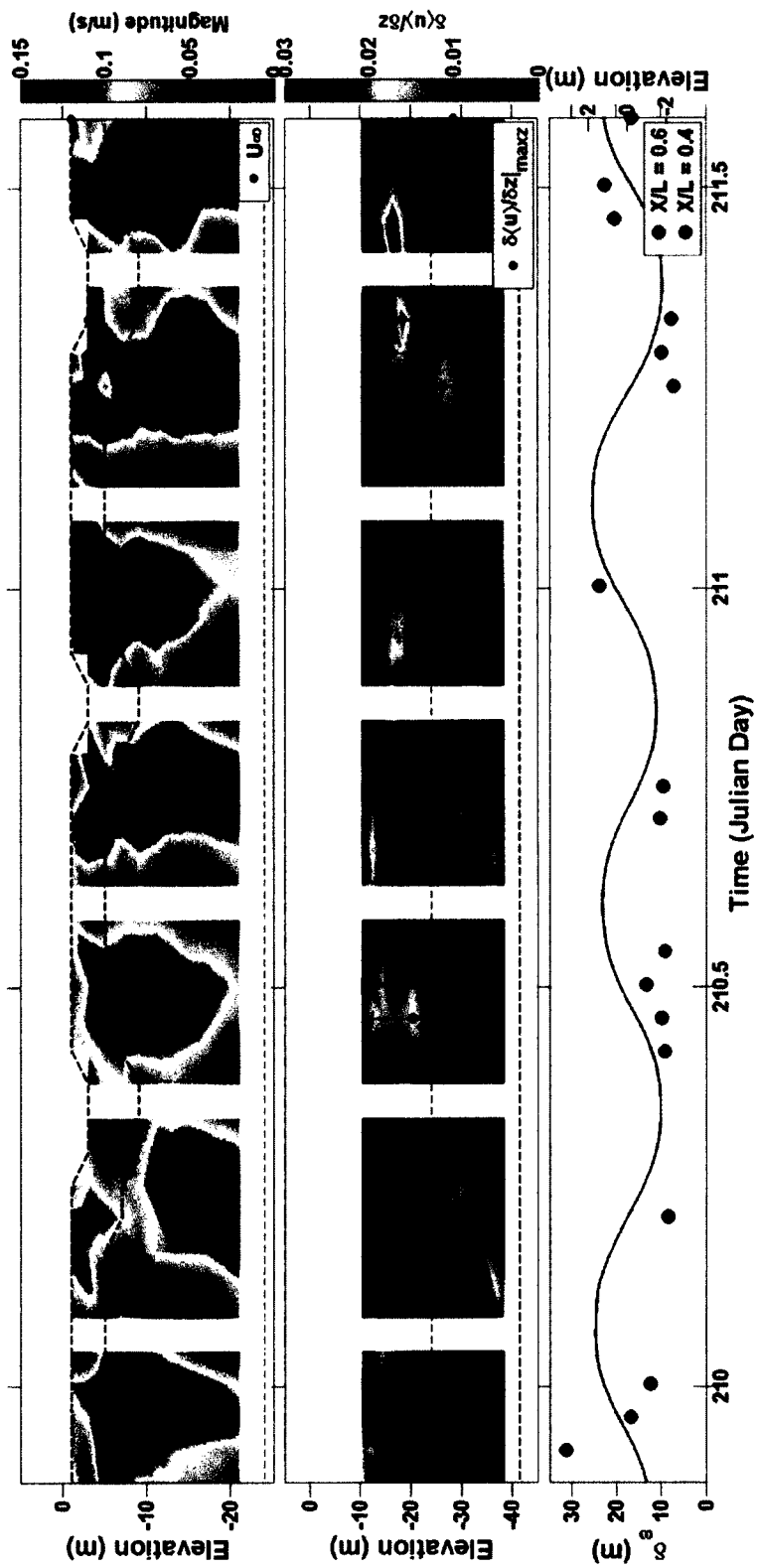
Figure 3-6. Vorticity thickness estimations over the southern pockmark. This figure has the same layout as Figure 3-5.

58
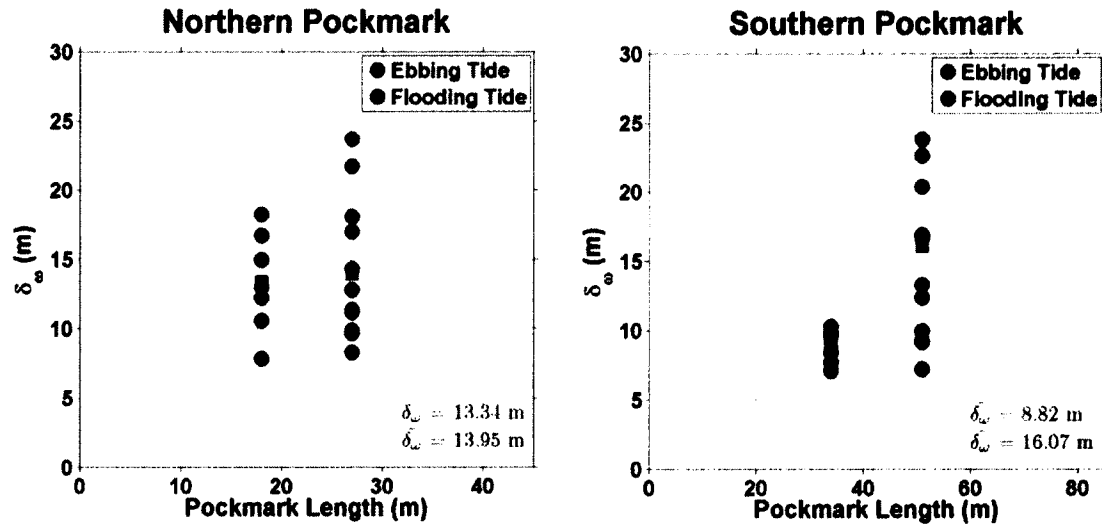
Figure 3-7. Vorticity thickness relative to pockmark length estimated over the northern and southern pockmark during flooding (blue) and ebbing (red) tidal conditions. Man vorticity thicknesses during flooding and ebbing tidal conditions are represented as black squares and displayed in the lower right corner of each graph.

Hydrodynamic modeling of flow within a pockmark obtained by Hammer, *et al.* (2009) and Brothers, *et al.* (2011b) were qualitatively compared to the cavity flow model to further assess the applicability of this model in predicting pockmark flow circulation patterns. Hammer, *et al.* (2009) conducted three-dimensional numerical simulations of flow within a pockmark (L/D = 5.7) and found contour-following horizontal velocity currents that decreased in magnitude with depth, representative of closed cavity flow. Their length-to-depth ratio of the modeled pockmark is close to the theoretical threshold of open cavity flow (L/D <6) and may explain the observed inconsistencies.

Numerical simulations conducted by Brothers, *et al.* (2011b) examined circulation patterns arising from two-dimensional turbulent flow over a shallow pockmark (L/D ≈ 18) and three-dimensional laminar flow over a deep pockmark (L/D ≈ 4.7). Modeled

59

results indicate contour-following currents within the shallow pockmark and the formation of a large circulation cell within the deep pockmark that bridges the pockmark opening and circulates throughout the depression. These results are consistent with cavity flow circulation that predicts contour-following currents in shallow (L/D <6) cavities and recirculation cell formation within deep cavities (L/D > 9). The consistency between modeled and empirical results of Belfast Bay pockmark flow patterns and cavity flow circulation suggest that cavity flow circulation may be a good first-order model of pockmark flow circulation.

2.6 Conclusions

Horizontal current direction profiles acquired over the near-center of two pockmarks in Belfast Bay show significant rotation with depth that exhibits a tidally-modulated pattern, specifically below the rim. During the flooding tide, nearly northward surface currents gradually rotate 75 ± 25 *deg* with depth. Larger directional changes are observed during ebbing tidal flow on the order of 180 ± 50 *deg* and typically occur abruptly around 10 *m* from the bottom. These observations of a greater degree of rotation with depth during ebbing tidal conditions are qualitatively consistent with circulation patterns predicted by open cavity flow.

Open cavity flow typically occurs in deep cavities (L/D < 6) and is characterized by shear layer growth with distance downstream. Shear layer growth rates were approximated using vorticity thickness and are positive across both pockmarks. These observations of near-bed flow reversal and shear layer growth with distance downstream

are consistent with open cavity flow patterns and suggest that pockmark flow circulation in Belfast Bay may be represented by cavity flow.

Future pockmark circulation studies should complete long-term measurements of the horizontal and vertical velocity structure at multiple locations within the depression in order to better resolve three-dimensional flow patterns within pockmarks. Modeling efforts should investigate the influence of varying pockmark geometry (*e.g.* symmetry and L/D ratios.), pockmark density, and internal pore water and gas excavation on regional and local flow patterns of pockmarks.

CHAPTER 4

OBSERVATIONS OF POCKMARK FLOW STRUCTURE IN BELFAST BAY, MAINE, PART 3: IMPLICATIONS FOR SEDIMENT TRANSPORT

4.1 Abstract

Current observations and sediment characteristics acquired within and along the rim of two pockmarks in Belfast Bay, Maine, were used to characterize periods of incipient motion and to investigate conditions favorable to the settling of suspended sediment. Observations were obtained over a 4-day period in late July of 2011 during average tidal and benign wave and wind conditions in water depths ranging 21 (32) to 25 (41) m at the rim (center) of each respective pockmark. The critical Shields parameter was approximated with the theoretical model of Dade, $et\ al.$, (1992) that characterizes the cohesive forces between individual sediment grains using the yield stress of the sediment. Hourly-averaged Shields parameters determined from horizontal current velocity profiles within the center of each pockmark never exceed the critical Shields parameter. However, stronger currents along the pockmark rims are consistent with conditions that support incipient motion and sediment suspension near the bed. The critical Shields parameter was periodically exceeded along the rim of each pockmark during maximum ebb and flood tidal flows, particularly at the southern pockmark where higher-velocity horizontal currents were observed. Depth-averaged vertical velocities at the ADCP below the rim in

the near-center of each pockmark were less than zero (downward) nearly 60% (55%) of the time in the northern (southern) pockmark and are often comparable in magnitude to corresponding depth-averaged horizontal velocities below the rim. At the rim of each pockmark, depth-averaged vertical velocities over the lower 8 m of the water column are also primarily negative, but of much lower magnitude than the corresponding depth-averaged horizontal velocities. Therefore suspended sediment may be moved to a distant location, resulting in bed erosion at the rim. Although infrequent, during periods of positive depth-averaged vertical velocities over the rim and center of each pockmark, estimated maximum grain sizes capable of remaining in suspension under terminal settling flow conditions, were much greater than the observed median grain diameter at the bed. Therefore, during upwelling flow within the pockmarks, and in the absence of flocculation, suspended sediment would not settle through the water column and may be moved downstream. The greater frequency of observed conditions that predict incipient motion along the rim of the southern pockmark is consistent with pockmark morphology in Belfast Bay which transitions from more spherical to more elongated with distance offshore. Observations of both incipient motion along the rim and conditions that support both deposition or continued suspension of sediment in the center of either pockmark suggest near-bed sediment transport may contribute to post-formation pockmark evolution during average, benign conditions in Belfast Bay.

4.1 Introduction

Pockmarks are large, circular to elongate seafloor depressions and are globally distributed in a wide-range of settings including estuaries (Scanlon and Knebel, 1989; Barnhardt, *et al.*, 1997), lakes (Pickrill, 2006; Manley, *et al.*, 2004), and offshore

environments (King and MacLean, 1970; Paull, *et al.*, 2002). Pockmarks range in size from a few meters to several kilometers in diameter and form from a sudden or gradual release of fluid and gas from underlying sediment (Judd and Hovland, 2007). In minimally-venting pockmark fields, flow-induced turbulence and low sediment input are typically invoked as mechanisms of post-formation pockmark maintenance, yet few studies have numerically modeled current flow within pockmarks (*e.g.*, Hammer, *et al.*, 2009; Brothers, *et al.*, 2011b) or obtained physical measurements within these depressions (*e.g.*, Manley, *et al.*, 2004).

Field observations and numerical modeling of current flow over a spherical pockmark (Hammer, *et al.*, 2009) indicate upwelling and flow recirculation within the depression that is qualitatively consistent with a theoretical model proposed by Manley, *et al.* (2004). The model describes the formation of a cyclostrophic rotational flow within the pockmark due to the elongation of the water column over the depression. This circulation pattern may prevent the settling of fine-grained material within the pockmark (Hammer, *et al.*, 2009), which is consistent with observations of coarser-grained deposits within the center of many pockmarks (*e.g.* Manley, *et al.*, 2004; Webb, *et al.*, 2009). A subsequent study (Brothers, *et al.*, 2011b) examined uni-directional flow over a spherical pockmark through numerical modeling and flume-tank experiments and observed enhanced turbulence along the rim and base of the depression. Recent field observations obtained in estuarine pockmarks located in Belfast Bay, Maine, show that strong overturning events extending from the rim to the bottom of the pockmark occur periodically (Chapter 2 of this thesis), and that horizontal circulation and shear layer thickness evolution across the pockmark are qualitatively consistent with open cavity

flow (Chapter 3 of this thesis). These observations suggest that near-bed turbulence induced by bottom shear stresses and circulation in the pockmark may lead to net sediment transport and contribute to long-term maintenance of pockmarks in Belfast Bay.

This study examines hydrodynamic processes and sediment properties within and around two pockmarks in Belfast Bay using field observations of currents and sediment characteristics obtained within the center and along the rim of these depressions during a rising high tide (Figure 4.1). Belfast Bay is located in the northwestern Gulf of Maine, approximately 20 *km* southwest of the Penobscot River (346 m^3/s^2 mean discharge; PEARL, 2011) and is characterized as a shallow, estuarine environment. Pockmark morphology in Belfast Bay varies from more circular in the north to more elongated in the south where the bay constricts in width from 8.5 *km* to 2.6 *km*. Evidence exists both for and against an actively venting pockmark field in Belfast Bay. Observations of acoustic turbidity (Brothers, *et al.*, 2011a), sidewall angles in excess of the angle of repose (Brothers, *et al.*, 2011b), and material being ejected from a pockmark (Kelley, *et al.*, 1994) provide evidence for actively degassing pockmarks in Belfast Bay. However, a recent geochemical survey of Belfast Bay reported no evidence of active methane or pore-fluid excavation and concluded that the Belfast Bay pockmarks may be inactive (Ussler, *et al.*, 2003). This paper shows that flow-induced stress may act to modify the Belfast Bay pockmarks in conjunction with, or in the absence of natural gas and pore-water excavation.
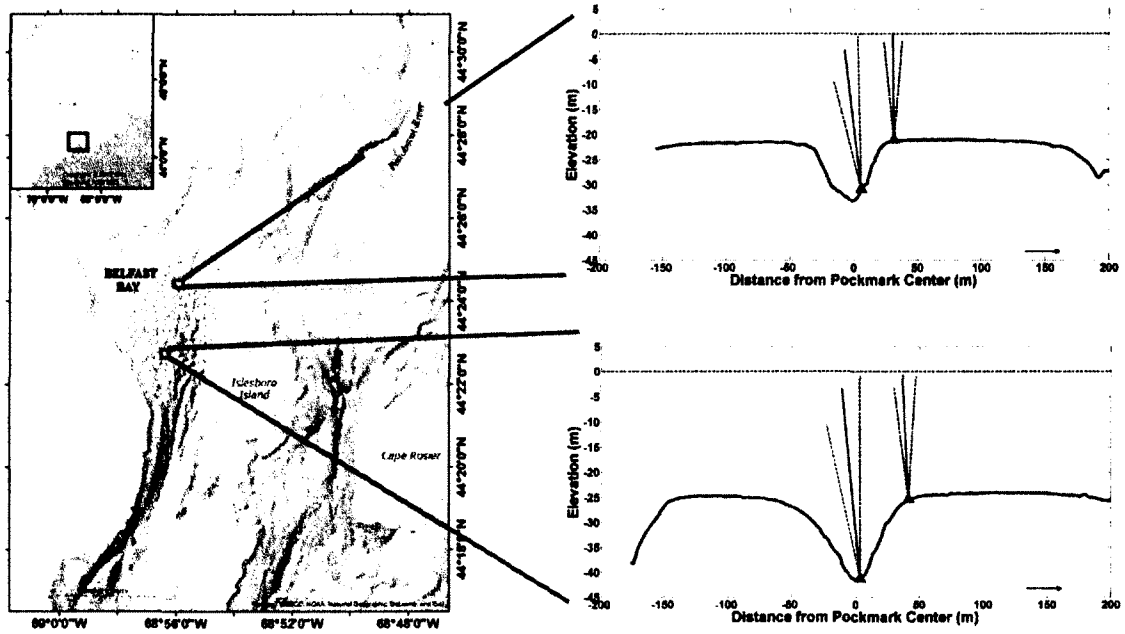
Figure 4.1. Locations of the sampled northern and southern pockmarks in Belfast Bay, Maine. Right panel shows the north-south bathymetric profile (black line) across the northern (upper) and southern (lower) pockmark with x-axis indicating distance from the pockmark center and y-axis showing elevation relative to mean sea level. The dashed blue line denotes the surface. Gray triangles represent the approximate locations of the ADCP mounts with extended dashed lines showing the acoustic beam angles. Note, current measurements were eliminated at depths that were not reached by all acoustic beams.

4.1.1 Sediment Transport

Sediment transport of unconsolidated sediments on the seafloor is often parameterized by the Shields parameter, θ, given by

$$\theta = \frac{\rho u_*^2}{(\rho_s - \rho)g d_{50}}$$ (4-1)

where ρ is the density of water, ρ_s is sediment density, g is gravity, d_{50} is the median grain diameter, and u_* is the friction velocity. The Shields parameter characterizes the ratio of the quadratic bed shear stress gradient, $\frac{\tau_b}{d_{50}} = \rho u_*^2$, to the immersed weight of the sediment, $(\rho - \rho_s)g$. Under turbulent flow conditions, as observed over the sampled pockmarks (Chapter 2), a logarithmic velocity profile is typically used to characterize the near-bed, time-averaged horizontal velocity profile and to estimate the temporarily varying friction velocity. Following Whitehouse, et al., (2000), under hydrodynamically smooth flow conditions, as are typically found in muddy estuaries (with $d_n < 62.5 \ \mu m$) like Belfast Bay, the logarithmic velocity profile varies as a function of u_* and height, z, above the bottom, and is given by the equation,

$$\frac{U(z)}{u_*} = 5.5 + 2.5 \ln\left(\frac{u_* z}{v}\right), \qquad \frac{u_* k_s}{v} \leq 5$$ (4-2)

where $U(z)$ is the mean horizontal velocity profile above the bed, υ is the kinematic viscosity of water, and $k_s = 2.5d_{50}$ is the Nikuradse roughness. Estimates of u_* can be obtained from (4.2) through iteration and using the value of $U(z)$ at the closest near-bed location (assuming a logarithmic profile extending from the bed).

Incipient motion represents the instant when an individual sediment grain begins to move. For incipient motion to occur, the Shields parameter must exceed a critical value, $\theta > \theta_{cr}$, where

$$\theta_{cr} = \frac{\rho u_{*cr}^2}{(\rho_s - \rho)g d_{50}} \tag{4-3}$$

and u_{*cr} is the critical friction velocity. The critical Shields parameter is typically estimated using the empirically-based Shields diagram. However, when sediment exhibits cohesive properties, the critical Shields parameter must account for the cohesive bonds between individual sediment grains. Dade, *et al.* (1992) formulated a theoretical model to approximate the critical Shields parameter for cohesive sediment as a ratio of the gravitational, frictional, and cohesive properties acting to keep a grain stationary in the presence of lift and drag forces imposed by the overriding, near bed flow. In their model, the cohesive force between particles per surface area of grain is represented by the yield stress, which has been empirically correlated to the critical bed shear stress by Mignoit (1968). Assuming the viscous region of the overriding turbulent flow is large relative to

68

the spherical grain size, Dade, *et al.* (1992), showed that the critical Shields parameter (θ_{cr}) for mud may be approximated by,

$$\theta_{cr} = \frac{\frac{\pi}{b_1 48}\tan(\varphi)}{1+0.1(Re_*)_{cr}\tan(\varphi)}\left(1 + \frac{F_A}{F_S}\right), \quad (Re_*) < 3 \qquad (4\text{-}4)$$

where

$$b_1 = \frac{\sqrt{1 - R^2}}{R^{1/3}\cos^{-1} R}$$

$$\frac{F_A}{F_S} = 3b_2(1 - \cos\varphi)\frac{\tau_y}{g(\rho_s - \rho)d_{50}}$$

$$b_2 = \left(\frac{R}{18}\right)^{1/3}\left(2 + \frac{1}{R}\right)$$

and Re_* is the Reynolds number given by its critical value, $(Re_*)_{cr}$,

$$(Re_*)_{cr} = \frac{(u_*)_{cr}d_{50}}{\upsilon} \qquad (4\text{-}5)$$

The angle of repose (φ) of the sediment was approximated as 20 *deg*, typical of fine-grained marine sediment (Booth, *et al.*, 1985). The shape factor b_1 relates the drag force acting on the particle relative to the drag force acting on a sphere of equivalent volume, under the assumption that R, the characteristic aspect ratio of cylindrical grains, is less than one. The characteristic aspect ratio ($R = 0.8$) was estimated from scanning electron microscope images of sediment collected in the western Gulf of Maine by Mazzullo, *et*

69

al. (1988). The shape factor b_2 is also a function of the characteristic aspect ratio, R, and accounts for the platiness of the particle. The ratio F_A/F_g relates the net interparticle cohesive force acting in the vertical (F_A) to the submerged particle weight induced by gravity (F_g), and is a function of the yield stress, τ_y, of the surficial, fine-grained sediment. The yield stress of remolded sediment is typically and most directly measured using a controlled stress rheometer (Van Kessel and Blom, 1998), and was empirically related to the measured moisture content of the soil, W, by Hoepner, *et al.*, (2001) by

$$\tau_y = 5.75 - 1.84W \tag{4-6}$$

Substitution of (4.5) into (4.4) and using (4.3) – (4.6) yields a cubic equation in $u_{*_{cr}}$ that can be solved analytically, with the single real root being the solution of interest. The critical friction velocity can then be substituted into (4.3) to yield the critical Shields parameter that defines a threshold over which cohesive sediment is expected to move.

For sediment to settle out of suspension, the sediment settling velocity must be greater than the depth-averaged vertical velocities, w, near the bed. When depth-averaged vertical velocities are negative and comparable in magnitude to the depth-averaged horizontal currents, suspended sediment will settle at a rate that varies with sediment grain size and density. Conversely, when depth-averaged vertical velocities are positive, settling will only occur if the settling velocity of an individual particle is greater than the upwelling vertical velocities. The terminal settling velocity of a particle is reached when the downward force induced by gravity is counteracted by the resistive

force induced by the fluid's drag. Stoke's law (Winterwerp and Van Kesteren, 2004) defines the terminal settling velocity, V_s, in terms of the particle diameter d_n,

$$V_s = \frac{(\rho_s - \rho)g d_n^2}{18\mu} \tag{4-7}$$

where μ is the dynamic viscosity of water. The maximum grain diameter capable of remaining in suspension under the observed flow conditions, $d_{n_{max}}$, can be determined by substituting the observed depth-averaged vertical velocities, w, for the terminal settling velocity, V_s, and solving for $d_{n_{max}}$, where,

$$d_{n_{max}} = \sqrt{\frac{18\, w\mu}{(\rho_s - \rho)g}} \tag{4-8}$$

Comparison of $d_{n_{max}}$ to the observed median grain size, d_{50}, of the bed sediment provides some indication whether sediment would be expected to settle out in the presence of the observed vertical velocities.

It should be noted that (4.8) was developed for non-cohesive sediments, and does not account for fine-grained sediment deposition through flocculation. The degree of flocculation is controlled by a variety of sediment and flow characteristics including the size, concentration, and physical and chemical properties of the suspended material as well as the dimensions of the smallest turbulent eddies within the flow (Van Leussen, 1988; Manning, et al, 2011). Nonetheless, when depth-averaged vertical velocities are greater than 0 m/s (i.e., upwelling conditions), the likelihood of unconsolidated sediment

71

settling out of suspension can be qualitatively evaluated by estimating $d_{n_{max}}$ from (4.8) and comparing these values to the observed d_{50}.

4.2 Methods

The theoretical development above indicates that estimations of the critical Shields parameter and maximum grain size under terminal settling conditions requires observations of the local horizontal and vertical currents ($U(z)$ and $w(z)$) and sediment characteristics (W and d_n). The vertical profile of the horizontal and vertical currents as well as sediment water content and grain size distribution were measured at the rim and center of two pockmarks in Belfast Bay to characterize periods of incipient motion and sediment settling over a 48 hr sampling period in late July 2011. The sampled pockmarks consist of a shallow, nearly circular, 45 m diameter pockmark with 12 m of relief located in the northern region of the bay and a deeper, more elongated, 85 m diameter pockmark with 17 m of relief located further south (Figure 4.1). Current velocity profiles were obtained at the rim and center of each pockmark using upward-looking 300 kHz RDI Workhorse Acoustic Doppler Current Profilers (ADCPs) mounted on an aluminum frame. Data were collected through a vertical column beginning 2.37 m (rim) and 2.24 m (center) above the seafloor and averaged spatially over 4 successive 0.5 m bins and temporally over 1 hr intervals. The center current meter mount additionally housed a Nortek Aquadopp current meter positioned 0.7 m above the seafloor that sampled hourly-averaged near-bed currents. Details of the ADCP deployments and survey methods are described in detail in Chapters 2 and 3 of this thesis. This study will focus on the horizontal and vertical current velocities averaged over the mid-water column, from 8 m

to the rim depth, and the deep-water column, from the rim depth to the bottom of the pockmark.

Sediment samples were obtained from the center and rim of each pockmark using a Shipek grab sampler and were placed in sealed, quart-sized plastic bags. After acquisition, samples were analyzed for water content and grain size. Water content measurements were made in July 2012 by measuring the loss of mass between a wet, m_{wet}, and then oven-dried, m_{dry}, sample, following standard procedures (ASTM Standards, 2010). Data are presented as a percentage of the sample's dry mass ($W = (m_{wet} - m_{dry})/m_{dry}$). Although water content measurements were completed nearly 12 months after data collection, the effects of evaporation are expected to be minimal due to the placement of the sediment samples in sealed, plastic bags and a controlled environment. Next, sediment samples were prepared for sediment grain size analysis and placed in 100 mL beakers filled with a 3% Hydrogen Peroxide solution for 60 days to decompose all organic matter. Prior to analysis, individual sediment samples were disaggregated using an ultrasonic disintegrator. Particle size distribution was then measured using the LS 13 320 laser diffraction particle size analyzer at the Woods Hole Oceanographic Institution Reinhart Coastal Research Center.

4.3 Results

4.3.1 Sediment Characteristics

Water content measurements were made from 4 sediment samples obtained at the rim and center locations of each pockmark (Table 1). Measured water content values ranged from 155 – 212% by weight and typically, in 3 of 4 cases, varied by less than 5% between the two samples obtained from the same location. Although a larger variation (about 30%) in water content values was observed from samples obtained at the center of the southern pockmark, the fractional error is within about 15%. These measurements are comparable to values of water content made by Hoepner, *et al.* (2001) from sediment with similar characteristics to the Belfast Bay sediment. Yield stress (τ_y) estimates were calculated from mean water content values at each location using (4.6), following Hoepner, *et al.*, (2001), and are also summarized in Table 1.

Table 4-1. Water content (W), yield stress (τ_y), median grain diameter (d_{50}) and critical Shields parameter (θ_{cr}) estimates obtained at the rim and center of the northern (upper panel) and southern pockmark (lower panel). Uncertainty measurements represent the range of variability observed between measured water content values from sediment obtained at the same location.

		W (%)	τ_y (N/m^2)	d_{50} (μm)	θ_{cr}
Northern Pockmark	Rim	155.64 ± 1.06	2.88± 0.03	7.65	0.19± 0.001
	Center	154.89 ± 0.98	2.90 ± 0.01	7.28	0.20 ± 0.001
Southern Pockmark	Rim	167.56 ± 4.27	2.67± 0.08	7.06	0.19 ± 0.004
	Center	212.35 ± 30.11	1.84± 0.56	6.33	0.15± 0.04

Sediment grain size distribution was measured at both the rim and center of each pockmark, and is shown in Figure 4.2 as a function of grain size (in μm) and percent volume concentration. Median grain size (d_{50}), shown in Table 4-1, ranged from 6.33 – 7.65 μm and is representative of fine, silty muds. Sampled sediments are assumed to have a sediment density (ρ_s) of 2173 kg/m^3 based on sediment density measurements acquired from near-by sediment in Sommes Sound, Mt Desert Island by Gschwend and Hites (1981). Total organic matter measurements were not made in this study.
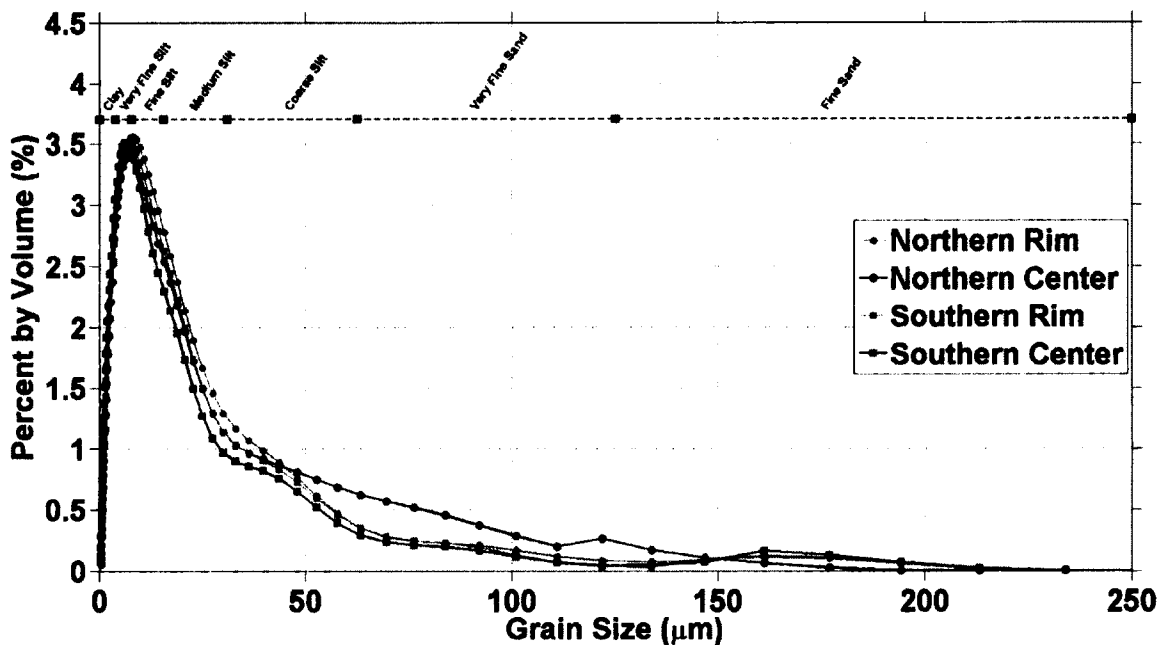
Figure 4-2. Sediment distribution of samples collected at the rim (gray) and center (black) of the northern (circle) and southern (square) pockmarks as a function of grain size and percent volume. Grain size classification and delineation is according to Wentworth (1922).

4.3.2 Currents

Figure 4.3 shows the observed hourly and depth-averaged horizontal and vertical velocities as a function of tidal phase at the rim and center of each pockmark. Current data were acquired during the rising high tide and therefore represent average tidal conditions. Mid-water currents are averaged over the depth interval ranging from 8 m below the surface to the depth of the rim and deep-water currents are averaged over the depth interval ranging from the depth of the rim to the bottom of the pockmark. Mid-water flow is strongly tidally modulated with maximum velocities occurring during mid tidal phases. Mid-water horizontal currents are typically of the same order of magnitude during maximum flooding and ebbing tidal conditions and range from 0.03 - 0.17 m/s. Mid-water vertical velocities are nearly always less than zero, with maximum currents reaching -0.01 m/s. Positive vertical velocities are temporarily observed during maximum flooding tide, but do not exceed 0.005 m/s. Overall, mid-water column vertical velocities are less than zero 85% of the time and are consistently much less than the corresponding depth-averaged horizontal velocities.

Depth-averaged horizontal velocities below the rim range in magnitude from 0.01-0.08 m/s and reach maximum velocities at mid-tidal phases. Compared to depth-averaged horizontal velocities above the rim, deep-water currents are weaker and less tidally influenced. Vertical velocities below the rim are comparable in magnitude to the deep-water horizontal flows and range from -0.02 – 0.02 m/s, with a tidally modulated pattern that shows periods of strong upwelling and downwelling (discussed in more detail in Chapter 2). Hourly-averaged deep-water vertical velocities are negative 72% of the time during the northern pockmark sampling period and 81% of the time during the southern

pockmark sampling period. Therefore, vertical flow conditions below the rim at the location of the center current meter mounts may be primarily characterized by downwelling current velocities.
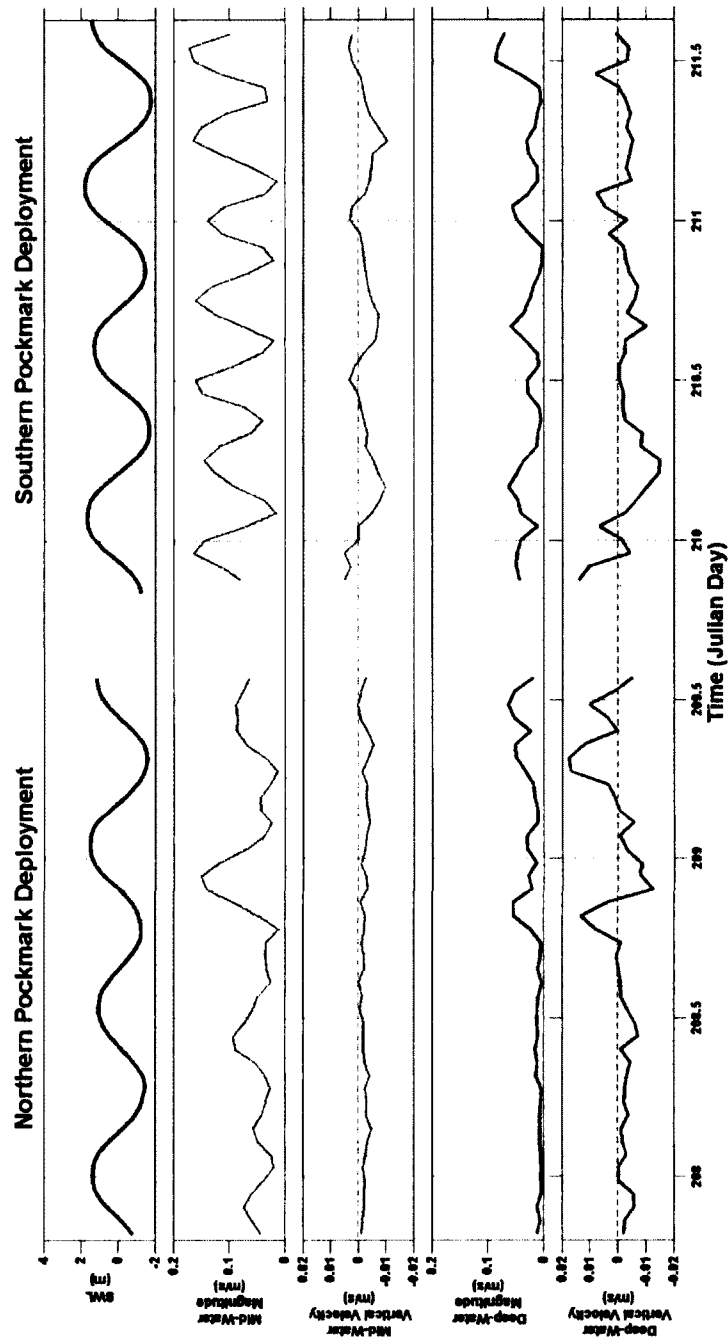
Figure 4.3. Depth-averaged mid-water and deep-water current magnitudes and vertical velocities observed at the rim (gray) and center (black) of each pockmark with time (Julian Days) on the x-axis. Upper panel shows mean sea surface elevation from bottom pressure data. Panels 2 and 3 show magnitude and vertical velocities measurements observed over the rim and depth-averaged from 8 m below the surface to the depth of the rim. Panels 4 and 5 show magnitude and vertical velocity measurements observed over the center and depth-averaged from the rim depth to the bottom of the pockmark.

79

The ratio of the depth-averaged vertical currents (w) to the corresponding horizontal currents $\left(\sqrt{u^2 + v^2}\right)$ over the rim and center of each pockmark are displayed in Figure 4.4 as a function of depth. When $-1 < \frac{w}{\sqrt{u^2 + v^2}} < 1$, the depth-averaged horizontal current magnitude is greater than the corresponding vertical velocities, and when $-1 > \frac{w}{\sqrt{u^2 + v^2}} > 1$, the opposite is true. Overall, the ratio of the depth-averaged vertical velocities relative to the corresponding horizontal currents increases and becomes more negative with depth. Above the rim, depth-averaged horizontal current magnitudes are typically much stronger than the corresponding vertical velocities, but decrease with depth relative to the negatively increasing vertical velocities. At the near-center ADCP location, above the rim, depth-averaged horizontal currents are strong relative to the corresponding vertical velocities. Below the rim, $\frac{w}{\sqrt{u^2 + v^2}}$ negatively increases. Within about 10 m of the bed, vertical velocities significantly increase relative to the corresponding horizontal current velocities and become comparable in magnitude. Multiple hourly-averaged periods are characterized by stronger depth-averaged vertical velocities relative to the corresponding horizontal flows below the rim. The reason for the observed inconsistency between current measurements made by the ADCP relative to the Aquadopp at the near-center mount location (closest, near-bed measurement) is most likely due the presence of the acoustic release influencing the current measurements made by the Aquadopp current meter.
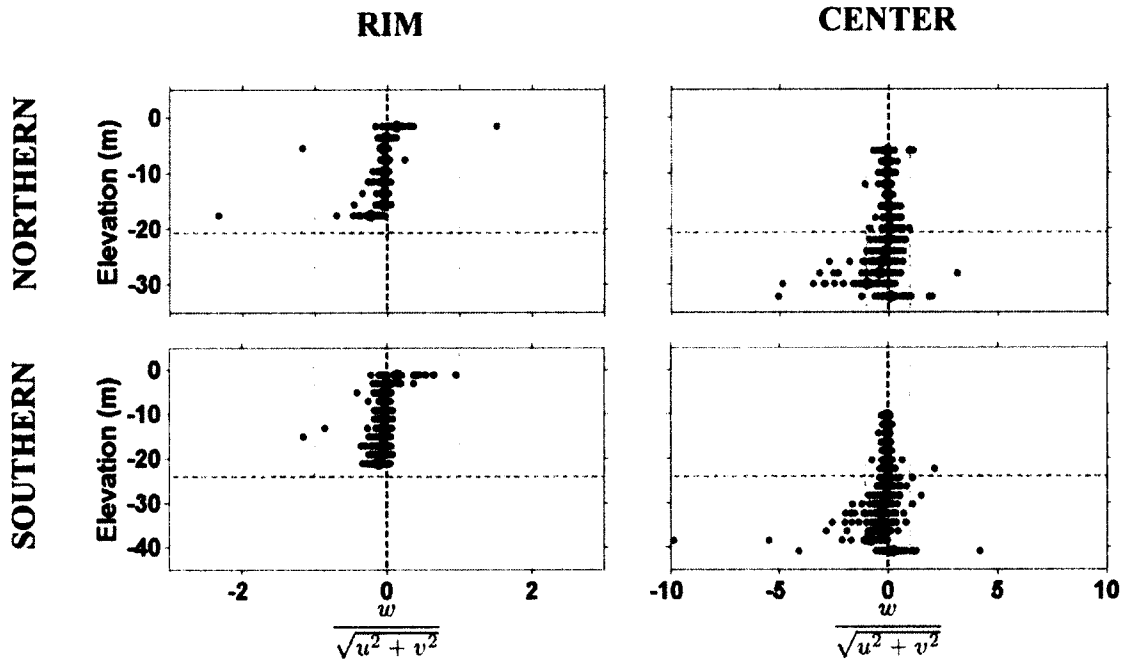
Figure 4.4. Depth-averaged vertical velocities relative to horizontal current magnitudes as a function of depth over the rim (left panel) and center (right panel) of the northern (upper panel) and southern (lower panel) pockmark. Black dots represent hourly-averaged ratios of the vertical velocities relative to the horizontal current magnitudes at each depth. Red dots show mean $\frac{w}{\sqrt{u^2+v^2}}$. The vertically dashed dark gray line show when $\frac{w}{\sqrt{u^2+v^2}} = 0$ and light gray vertically dashed lines denote $\frac{w}{\sqrt{u^2+v^2}} = \pm 1$.

Hourly-averaged friction velocities, u_*, were iteratively calculated using (4.2) and the observed time-averaged horizontal velocity closest to the bed. These friction velocities, in conjunction with the measured median grain size (d_{50}) and estimated sediment density (ρ_s) are used in (4.1) to estimate the Shields parameters, θ, for all time periods at both the rim and center positions of each pockmark when a logarithmic profile was observed in the hourly-averaged horizontal velocity profile (Figure 4.5). The estimated critical Shields parameter (θ_{cr}) was calculated using (4.3) – (4.5) as a function of the measured d_{50} and τ_y. Critical and hourly-averaged Shields parameter estimates at the rim and center of each pockmark are displayed in Figure 4.5 as a function of time. Critical Shields parameter estimates at each location are displayed in Table 4-1 with range estimates based on the range of measured water content values obtained from the sampled sediment at each location. Estimates of θ at the rim exceed the critical Shields parameter (θ_{cr}) several (9) times on the rising and falling tides, approximately corresponding to periods of maximum flow. The critical Shields parameter is more consistently exceeded at the rim of the southern pockmark on 5 out of 7 rising and falling tides, whereas at the rim of the northern pockmark, θ_{cr} is only exceeded on 1 out of 7 rising and falling tides. In total (including both sites), the critical Shields parameter is exceeded during 43% of the observed maximum flooding and ebbing tidal conditions. At the center current meter mount locations, θ is always much less than θ_{cr} and thus incipient motion is not predicted to occur in the near-center of the pockmarks during the observed tidal flows.
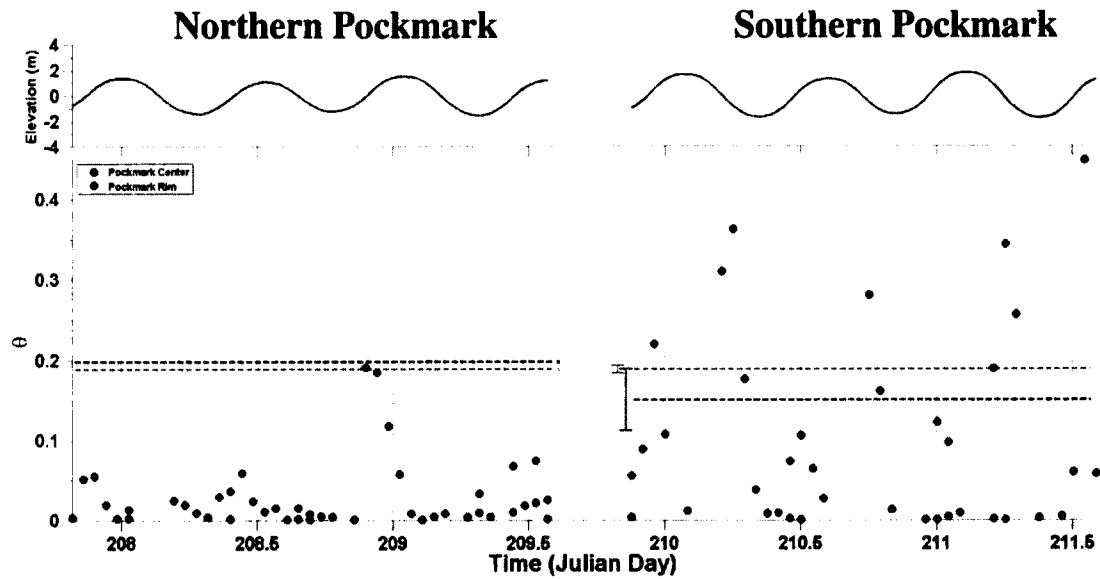
Figure 4.5. Shields parameter estimates for each hourly averaged period at the rim (gray) and center (black) of each pockmark as a function of tidal phase (upper panel. Dashed lines in the lower panel indicate the estimated critical Shields parameter at each location with error bars representing the range in critical Shields parameter estimates based on observed range in water content measured at each location. Note, hourly-averaged shields parameter estimates were only calculated when a logarithmic profile was observed in the corresponding hourly-averaged horizontal velocity profile.

Figure 4.6 shows the maximum grain diameter $(d_{n_{max}})$ capable of remaining in suspension given the observed positive mid-water and deep-water depth-averaged vertical velocities (w) at the rim and center mount locations, respectively. Mean median grain diameter (d_{50} = 7.05 μm) is also shown in figure 4.6. When negative vertical velocities are observed, all grains are predicted to settle towards the bed and $d_{n_{max}}$ were not estimated. During upwelling events, the estimated $d_{n_{max}}$ was always much larger than the median grain diameter, d_{50} and suggests that in the absence of flocculation, all entrained grains less than the maximum grain diameter $\left(d_{n_{max}}\right)$ will remain in suspension.

Flocculation, unaccounted for in the analysis completed in this study, is expected to strongly influence the flow regime and sediment characteristics within Belfast Bay based on the observed sediment grain size distribution and anecdotal evidence for significant organic matter within the sediments. Flocculation would result in enhanced sediment sizes and increased settling rates, particularly during prolonged periods of downwelling currents. Therefore, effective *in situ* grain diameters of suspended material are most likely larger than the median grain diameter used herin, and suggests that a greater amount of sediment deposition would be expected in the vicinity of the observed pockmarks under similar flow conditions to those observed during this field experiment.
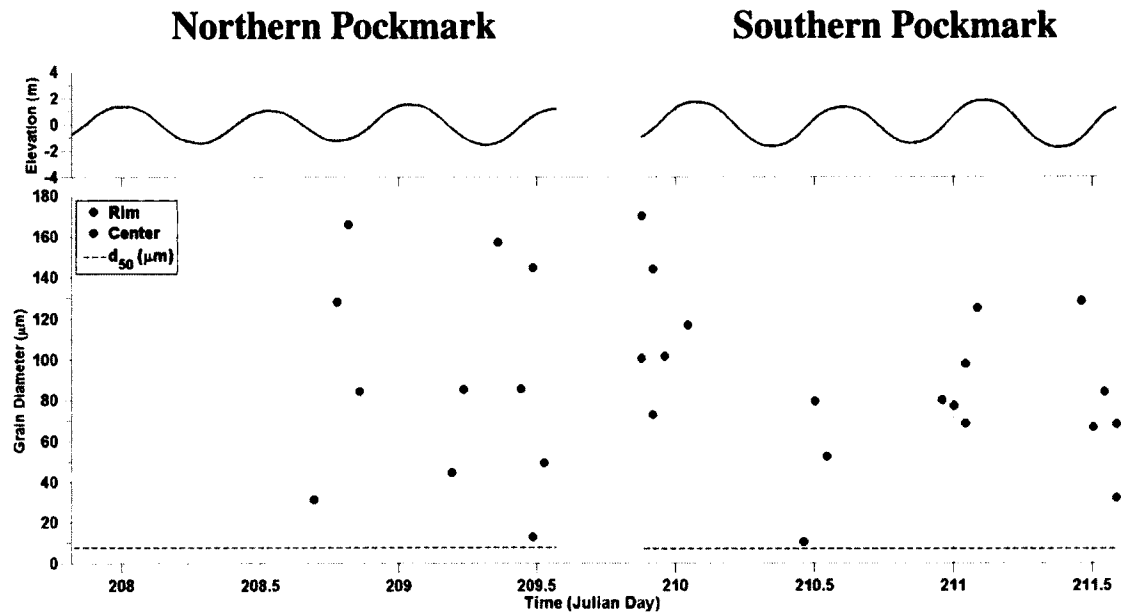
Figure 4.6. Estimated maximum grain diameters predicted to remain in suspension during observed positive vertical velocity events at the rim (gray) and center (black) of each pockmark as a function of time (upper panel). The dashed red line in the lower panel denotes the average median grain diameter of 7.05 μm. Highlighted regions indicate periods during which incipient motion is predicted to occur. Note, maximum grain diameter estimates under terminal settling conditions were calculated at the rim from positive depth-averaged mid-water vertical velocities and at the center from positive depth-averaged deep-water vertical velocities.

4.4 Discussion

Incipient motion occurs when the Shields parameters (θ) exceeds the critical value (θ_{cr}) and thus depends on the parameters that determine θ_{cr}. The estimated critical Shields (θ_{cr}) parameter is a function of many variables (φ, R, g, ρ_s, ρ, d_n, τ_y, υ, u_*), but in this study based on directly measured parameters, is most sensitive to variation in yield stress (τ_y) approximations. The linear equation used to calculate yield stress (τ_y) in this study was developed by Hoepner, *et al.* (2001). Their model is based on an empirical comparison of measured yields stresses, obtained using a rheometer, and water content values measured from estuarine sediment samples similar in grain size and water content to the sampled Belfast Bay sediment. Differences in water content observed between two measurements obtained at the same location (rim or center) of either pockmark agree to within 15% error. The range in measured water content values at each location is translated to estimates of the critical Shields parameter and is shown with error bars in Figure 4.5. However, because the estimated Shields parameters are often much greater than the critical value, our general conclusions regarding incipient motion remain unchanged.

4.4.1 Rim Sediment Transport

Estimates of θ along the rims of the northern and southern pockmarks are tidally modulated and greatest during the mid-tidal cycle periods (Figure 4-5). The overall weaker, less tidally-driven currents in the northern bay result in infrequent exceedance of

the critical threshold for incipient motion along the rim. A more consistent pattern of critical threshold exceedance is observed along the rim of the southern pockmark where stronger tidal currents were observed. Although tidal currents are stronger during the flooding tide, maximum bed shear stresses along the rim more consistently occur during the ebbing flow. This asymmetry may be related to the local circulation pattern and relative location of the current meter mounts (northern rim) with respect to the primary tidal direction. Field observations of pockmark rotational structure indicate flow reversal near the base of the pockmark and a greater degree of rotation during the ebbing tide (Chapter 3), consistent with open cavity flow models (Ashcroft and Zhang, 2005). Stream-wise (horizontally varying) velocity structure over an open cavity predicts greater shear at the upstream edge of the cavity than at the downstream location. Thus, a greater bed stress would be expected during the ebbing tidal flow due to the location of the current meter mount on the northern rim of either pockmark.

The maximum grain diameter under terminal settling conditions was estimated to assess the largest grain diameter capable of remaining in suspension under the observed positive depth-averaged vertical velocities and was always greater than the median grain diameter. This suggests that when incipient motion occurs simultaneously with a strong upwelling event above the rim, a large proportion of non-flocculated sediment eroded from the rim of the pockmark would stay in suspension. Such an event was recorded over two individual, hour-long periods at the rim of the southern pockmark and may characterize a period during which sediment is unable to settle through the water column. Conversely, simultaneous observations of incipient motion along the rim with downward-directed depth-averaged currents over the rim of the pockmark would characterize

periods during which sediment settles towards the bed and were observed 78% of the time during this sampling period. However, above the rim, the ratio of the depth-averaged vertical velocities to the corresponding horizontal currents negatively increases with depth and rarely exceeds ± 1. Therefore, close to the bed, the flow structure is primarily characterized by weak negative vertical velocities and stronger horizontal flows. As a result, during periods when incipient motion occurs simultaneously with downward-directed vertical velocities below the rim, suspended sediment may be transported downstream a distance before it is deposited.

4.4.1 Center Sediment Transport

In the center of each pockmark, θ never exceeded θ_{cr}, and near-bed sediment transport is not expected to occur during these average tidal flows. Furthermore, deep-water vertical velocities, comparable in magnitude to the depth-averaged horizontal velocities below the rim, are less than 0 (down-welling currents) 75% of the time. This suggests that on average, suspended sediments in the water column would tend to settle towards the bed. However, observations over the center of the pockmark of the ratio of the depth-averaged vertical velocities to the horizontal currents being greater than 1 at various depths below the rim in conjunction with estimated maximum grain diameters much greater than the median grain diameter at the bed, suggest that any suspended sediment below the rim during these time periods may potentially be transported out of the pockmark as a result of these strong upward-directed velocities .

4.4.3 Pockmark Maintenance

Pockmark morphology in Belfast Bay transitions from more spherical in the north to more elongated in the south and suggests that pockmark shape may not be exclusively controlled by vertical fluid escape. Maximum grain size estimations under terminal settling velocity conditions in excess of the median grain diameter in conjunction with observed periods of incipient motion along the rim of the southern pockmark, suggest that pockmark size and shape may be modified by near-bed sediment transport. The greater frequency of excess bed shear stress along the rim of the more southerly located pockmark is consistent with the elongated morphology of the pockmarks in the southern region of Belfast Bay. Similar observations of pockmark morphology transitioning from spherical to more elongated with distance offshore are found in Blue Hill Bay, Maine, and Passamaquoddy Bay, New Brunswick, Canada (Brothers, *et al.,* 2012) and may be related to fine-grained sediment erosion induced by excess bed shear stress along the rims of the pockmarks.

Although near-bed sediment transport is observed along the rims of each pockmark, incipient motion is never predicted to occur at the near-center of the pockmarks. Observations at the center of each pockmark of primarily negative (downward-directed) vertical velocities below the rim in conjunction with the critical Shields parameter never being exceeded suggest that the sampled pockmarks would fill in over time under similar conditions. However, these pockmarks have persisted for up to 11,000 years (Brothers, *et al.,* 2010). Potential mechanisms to explain the preservation of these large depressions over long time periods, may be related to the influence of strong upwelling events or local storm events enhancing sediment transport within pockmarks. Strong upwelling

events below the rim, as observed in this study, may advect suspended sediment out of the pockmark and more or less balance the net sediment deposition occurring during downwelling periods below the rim. Alternately, pockmark maintenance may be primarily controlled by sediment transport induced by higher-velocity flow due to spring tides or storm events, rather than during the average tidal current conditions during our sampling period. The influence of these higher flow conditions is not considered herein, but is the subject of ongoing research.

4.5 Conclusions

Observations of time-averaged horizontal and vertical velocity profiles were obtained with bottom-mounted ADCPs at the rim and in the near-center of two pockmarks in Belfast Bay, Maine, over a 48 hour period in late July 2011. Additionally, sediment grab samples were obtained at the rim and center of each pockmark to estimate the water content and median grain size at each location. The Dade *et al.* (1992) model predicts θ_{cr} for cohesive sediment using many physical properties of the sediment (*e.g.*, φ, R, ρ_s, d_n, τ_y). This study estimated φ, R, ρ_s, from data documented in the literature (Booth, *et al.*, 1985; Mazzullo, *et al.*, 1988, Gschwend and Hites, 1981). Future studies should obtain direct measurements of these variables to better constrain estimates of the critical Shields parameter. Observed currents were further averaged over the mid-water column, ranging from 8 *m* below the surface to the depth of the rim, and over the deep-water column from the rim to the bottom of the pockmark. Water content measurements ranged from 155 - 212% and were used to estimate sediment yield strength based on empirical formulations by Hoepner, *et al.* (2001). Sampled sediments, assumed to have a

density of 2173 kg/m^3 (after Gschwend and Hites, 1981), have mean grain diameters of 7.65 μm and are classified as silty muds. These current and sediment observations were used to estimate periods of incipient motion and to assess whether or not suspended sediment in the water column would settle under the observed flow conditions.

Shields parameter estimates, assuming hydrodynamically smooth flow, were made from observations of the near-bottom horizontal currents and the observed median grain size following Whitehouse, et al., (2000). The critical Shields parameter was predicted using the estimated yield stresses and the observed median grain diameter observed at the rim and center of each pockmark, following the theoretical model developed by Dade, et al. (1992) for cohesive sediments. Observed Shields parameters suggest that incipient motion regularly occurs during maximum flood and ebb tidal periods at the rim of each pockmark. The critical Shields parameter was more consistently exceeded at the rim of the southern pockmark where higher velocity flows were observed. Shields parameter estimates at the center of each pockmark were small and always less than the critical value, indicating that near-bed stress imposed by the overriding currents within the pockmarks was not significant enough to move sediment.

The relative magnitude of the horizontal and vertical velocities will determine the rate, distance, and direction that suspended sediment will be transported. Mid-water column vertical velocities are primarily negative and small relative to the observed horizontal velocities over this depth range. Therefore, sediment suspended at the rim is likely to be transported downstream. Below the rim, depth-averaged vertical velocities are negative 77% of the time and are comparable in magnitude to the horizontal flows.

Therefore, during down-welling periods below the rim, a large proportion of the suspended sediment would settle towards the bed.

During the infrequently observed positive vertical velocity events, sediment will remain in suspension unless the settling velocity exceeds the upward-directed flow. Using Stokes Law for grain settling (Winterwerp and Walther, 2004), the maximum grain diameter capable of remaining in suspension under the observed positive vertical velocities was calculated and was always greater than the median grain diameter at the bed. This suggests that in the absence of flocculation and during upwelling periods, sediment entrained into the flow would remain in suspension while the flow conditions persisted. It is important to note that the influence of flocculation is unaccounted for in this analysis and a greater degree of deposition is expected in the vicinity of the pockmarks due to the flocculation of material in the water column.

The greater frequency of critical Shields parameter exceedance observed at the rim of the southern pockmark qualitatively agrees with the observed pockmark morphology in Belfast Bay which becomes more elongated with progression southward. However, the majority of the sampling period is characterized by negative, depth-averaged vertical velocities and weak horizontal currents below the rim and strong mid-water horizontal currents. This suggests that a large proportion of the sampling period is characterized by the settling of suspended sediment in the center of the pockmark. Long-term pockmark maintenance may therefore be related to a larger amount of sediment being transported out of the pockmark during upwelling periods than is deposited during downwelling periods; however, this cannot be verified from the data collected in this study. Alternately, maintenance may be controlled by sediment transport induced by higher

velocity flow due to spring tides or storm events, rather than by the average tidal, wind, and wave conditions observed in this field experiment. Although this work presents evidence of incipient motion along the rim of the pockmarks during fairly mild conditions, longer term field observations such as these are needed to better determine the nature of the sediment transport in post-formation pockmark maintenance.

CHAPTER 5

CONCLUSIONS

Current and temperature and salinity observations over two sampled pockmarks in Belfast Bay, ME show evidence for internal mixing and overturning within the pockmark, circulation patterns that resemble open cavity flow, and incipient motion along the rims. Vertical current profiles were acquired at the rim and near-center of each pockmark using bottom mounted ADCPs over a 48 hour sampling period in late July 2011. Additionally, multiple CTD casts were acquired approximately every two hours over the near-center of each pockmark for a complete tidal cycle to examine the tidally-varying vertical structure over each pockmark. Sediment samples were also obtained at the rim and center of each pockmark to examine the grain size distribution and obtain water content measurements at each location. The sampled pockmarks consisted of a circular pockmark with a length-to-depth ratio of 3.7 and 45 m diameter in the northern region of the bay and a more elongated pockmark with a length-to-depth ratio of 4.7 and 85 m diameter in the southern region of the bay.

The observed vertical current structure over each pockmark was characterized by three distinct regions, the surface, middle, and deep layers, which were delineated by the average depth of the thermocline and rim depth. Surface and mid-water column currents are primarily tidally-driven, but show slight modifications by wind-driven flow. Below

94

the rim, low-velocity horizontal currents show significant rotational changes with depth. Depth-averaged vertical velocities over the near-center of each pockmark show strong upwelling and downwelling events that extend from above the rim down into the pockmark. These events are indicative of the interaction of flow above and below the rim. Evidence for mixing was further documented by salinity and temperature observations obtained from CTD casts over the near-center of each pockmark which showed uniform properties below 12 m. Individual, hourly-averaged horizontal velocity profiles over the center of each pockmark show multiple logarithmic regions. These observations are consistent with those obtained by Chriss and Caldwell (1982) and suggest form drag significantly influences the local flow regime. These vertical velocity and temperature observations suggest that the water column over the sampled pockmarks is characterized by active mixing and overturning of flow above and below the rim, while individual horizontal velocity profiles indicate that roughness-induced form drag significantly influences the local flow regime in the vicinity of the sampled pockmarks.

The tidally-varying rotational structure over the near-center of each pockmark is qualitatively consistent with circulation patterns predicted by open cavity flow. Significant directional changes were observed from surface to depth over each pockmark, specifically below the rim. During ebbing tidal conditions, abrupt directional changes were observed around 10 m from the bed and were typically on the order of 180 ± 50 deg. A more gradual change in direction from surface to depth was observed during flooding tidal conditions and was typically around 75 ± 50 deg. These observations of more abrupt and significant directional changes with depth during ebbing tidal flow are qualitatively consistent with open cavity flow and the formation of a recirculation cell within the

pockmark. Open cavity flow occurs in deep cavities, with length-to-depth ratios less than 6 and is characterized by shear layer growth with distance downstream. Because the current meter mounts positioned within the pockmark were located slightly north of the center, the thickness of the shear layer is expected to be greater during flooding tidal conditions. The time-mean behavior of the shear layer, approximated using vorticity thickness, was estimated from horizontal current magnitudes acquired over the near-center of each pockmark. Although the rate at which the shear layer grew across the depression differed between pockmarks, mean vorticity thickness estimates were greater during flooding tidal conditions and are therefore qualitatively consistent with open cavity flow. Numerical simulations completed by Brothers, *et al.* (2011b) examined circulation patterns within pockmarks and are qualitatively consistent with circulation patterns predicted by cavity flow. Our observations of rotational structure over each pockmark in conjunction with estimated shear layer growth across each depression suggest that cavity flow circulation may be a good first-order approximation of pockmark flow circulation.

Post-formation pockmark evolution and maintenance were investigated by characterizing periods of incipient motion and estimating conditions favorable to the settling of suspended sediment over each pockmark. Temporally-varying Shields parameter estimates were made assuming a hydrodynamically smooth flow and compared to the critical Shields parameter, estimated using the theoretical model proposed by Dade, *et al.* (1992) for cohesive sediment. A critical Shields parameter was estimated for the rim and center locations of each pockmark based on measured grain size and water content values obtained from sampled sediment at each location and estimated sediment

density, shape, and angle of repose. The critical Shields parameter was exceeded several times at the rim of each pockmark, typically during maximum velocity tidal periods and more consistently at the southern pockmark rim. At the center, the critical Shields parameter was never exceeded. The majority of the sampling period is characterized by downwelling below the rim and corresponding low-velocity horizontal currents. This suggests that the settling of suspended sediment within each pockmark would characterize the majority of the sampling period. At the rim, although also primarily characterized by downwelling flow, the corresponding horizontal currents are much stronger than the vertical velocities. Therefore, any suspended sediment is likely to be transported to a distant location. During the infrequent observations of upward-directed flow below the rim and directly above the rim, estimated maximum grain diameters capable of remaining in suspension under the observed vertical velocities are always much greater than the median grain diameter. This suggests that in the absence of flocculation, sediment would remain in suspension as long as these upwelling currents persisted. The more frequent exceedence of the critical Shields parameter at the rim of the southern pockmark is consistent with observations of more elongated pockmark morphology in Belfast Bay with progression seaward. Although multiple time periods are characterized by incipient motion, the majority of the sampling period is characterized by flow conditions favorable to deposition. Therefore, long-term pockmark maintenance in Belfast Bay may be more controlled by sediment transport induced by higher-velocity flows due to spring tides or storm events, rather than the average flows sampled in this study.

Future work should include long-term monitoring of the current and temperature structure at multiple locations within and around pockmarks in order to better understand the three-dimensional flow structure around these depressions. Field measurements should be conducted during storm events and spring and neap tides to assess the influence of these varying environmental conditions on the vertical structure over pockmarks and near-bed sediment transport. Sediment transport studies within the vicinity of pockmarks should acquire current measurements closer to the bed, floc size and settling rate estimates, as well as more detailed measurements of the physical properties of the sediment (*e.g.*, φ, R, ρ_s) in order to better constrain pockmark sedimentation and erosion rates. Measurements of floc size and settling velocity as well as the parameters that influence them may be achieved through use of multiple instruments including a digital floc camera, video settling column, optical backscatter sensor and current meter as described by Mikkelsen *et al.* (2004) and Fennessy *et al.*, (1994).

LIST OF REFERENCES

Ahuja, K., and Mendoza, J., 1995, Effects of cavity dimensions, boundary layer, and temperature on cavity noise with emphasis on benchmark data to validate computational aeroacoustic codes. NASA Contractor Report NASA CR 4653.

Andrews, B.D., Brothers, L.L. and Barnhardt, W.A., 2010, Automated feature extraction and spatial organization of seafloor pockmarks, Belfast Bay, Maine, USA. Geomorphology, v. 124, p. 55-64.

Arya, S.P.S., 1975, A drag partition theory for determining the large-scale roughness parameter and wind stress on the arctic pack ice. Journal of Geophysical Research, v. 80, p. 3447-3454.

Ashcroft G., and Zhang, X., 2005, Vortical structures over rectangular cavities at low speed. Physics of Fluids, v. 17, p. 1-8.

ASTM Standard D2216 – 10, 2010, Standard test methods for laboratory determination of water (moisture) content of soil and rock by mass, ASTM International, West Conshohocken, PA.

Barnhardt, W.A., Belknap, D.F., and Kelley, J.T., 1997, Stratigraphic evolution of the inner continental shelf in response to late Quaternary relative sea-level change, north-western Gulf of Maine. Geological Society of America Bulletin, v. 109, p. 612-630.

Booth, J.S., Sangrey, D., and Fugate, J., 1985, A nomogram for interpreting slope stability of fine-grained deposits in ancient and modern marine environments. Journal of Sedimentary Petrology, v. 55, p. 29-36.

Brothers, L.L., 2010, Nearshore pockmark field dynamics and evolution. PhD Dissertation, University of Maine, Orono, ME, 139 p.

Brothers, L.L., Kelley, J.T., Belknap, D.F., Barnhardt, W.A., Andrews, B.D. and Maynard M.L., 2011a, More than a century of bathymetric observations and present-day shallow sediment characterization in Belfast Bay, Maine, USA: implications for pockmark field longevity. Geo-Marine Letters, v. 31, p. 237-248.

Brothers, L.L., Kelley, J.T., Belknap, D.F., Barnhardt, W.A. and Koons, P.O., 2011b, Pockmarks: self-scouring seep features? Proceedings of the 7th International Conference on Gas Hydrates, Edinburgh, Scotland, United Kingdom, July 17-20.

Brothers., L.L., Kelley, J.T., Belknap, D.F., Barnhardt, W.A., Andrews, B.D., Legere, C., and Hughes Clarke, J.E., 2012, Shallow stratigraphic control on pockmark distribution in north temperate estuaries. Marine Geology, v. 329-331, p. 34-45.

Chriss, T.M., and Caldwell, D.R., 1982, Evidence for the influence of form drag on bottom boundary layer flow. Journal of Geophysical Research, v. 87, p. 4148-4154.

Christian, H.A., 2000, Gas sampling and seepage liquefaction assessment in Penobscot Bay, Maine, December 1999. Report to the Department of Geological Sciences, University of Maine. Christian Situ Geosciences, Halifax, Nova Scotia.

Christodoulou, D., Papatheodorou, G., Ferentinos, G., and Masson, M., 2003, Active seepage in two contrasting pockmark fields in the Patras and Corinth gulfs, Greece. Geo-Mar Letters, v. 23, p. 194-199.

Dade, W.B., Nowell, A.R.M., and Jumars, P.A., 1992, Predicting erosion resistance of muds. Marine Geology, v. 105, p. 285-297.

Fennessy, M.J., Dyer, K.R., and Huntley, D.A., 1994, INSSEV: an instrument to measure the size and settling velocity of flocs in-situ. Marine Geology, v. 117, p. 107-117.

Gay, A., Lopez, M., Ondreas, H., Charlou, J.L., Sermondadaz, G., and Cochonat, P., 2005, Seafloor facies related to upward methane flux within a giant pockmark of the lower Congo Basin. Marine Geology, v. 226, p. 81-95.

Gschwend, P.M., and Hites, R.A., 1981, Fluxes of polycyclic aromatic hydrocarbons to marine and lacustrine sediments in the northeastern United States. Geochimica et Cosmochimica Acta, v. 45, p. 2359-2367.

Hammer, Ø., Webb, K.E. and Depreiter, D., 2009, Numerical simulation of upwelling currents in pockmarks, and data from the Inner Oslofjord, Norway. Geo-Marine Letters, v. 29, p. 269-275.

Hoepner, M.A., 2001, Stability of cohesive sediments from flume and rheometer measurements. Unpublished MS Thesis, Georgia Institute of Technology, Atlanta, GA.

Hovland, M., and Judd, A.G., 1988, Seabed pockmarks and seepages: Impact on Geology, Biology, and the Marine Environment. London, Graham and Trotman Ltd, 293 p.

Hovland, M., 2005, Pockmark-associated coral reefs at the Kristin field off Mid-Norway. In: Freiwald, A., and Roberts, J.M. (eds.), Cold-water corals and ecosystems, Springer - Verlag, Berlin Heidelberg New York, p. 623-632.

Hovland, M., Svensen, H., Forsberg, C.F., Johansen, H., Fichler, C., Fosså, J.H., Jonsson, R., and Rueslåtten, H., 2005. Complex pockmarks with carbonate-ridges off mid-Norway: products of sediment degassing. Marine Geology, v. 218, p. 191-206.

Hovland, M., and Svensen, H., 2006, Submarine pingoes: Indicators of shallow gas hydrates in a pockmark at Nyegga, Norwegian Sea. Marine Geology, v. 228, p. 15-23.

Judd, A.G., and Hovland, M., 2007, Seabed Fluid Flow: Impact on Geology, Biology, and the Marine Environment, Cambridge University Press, Cambridge, 475 p.

Kelley, J.T., Dickson, S.M., Belknap, D.F., Barnhardt, W.A., and Henderson, M., 1994, Giant sea-bed pockmarks: evidence for gas escape from Belfast Bay. Geology, v. 22, p. 59-62.

King, L.H., and MacLean, B., 1970, Pockmarks on the Scotian Shelf. Geological Society of America Bulletin, v. 91, p. 3141-3148. Kranck, K., 1975, Sediment deposition from flocculated suspensions. Sedimentology, v. 22, p. 111-123.

Kundu, P., and Cohen, I., 2008, Fluid Mechanics, Elsevier Academic Press, 4th edition.

Manley, P.L., Manley, T.O., Watzin, M.C. and Gutierrez, J., 2004, Lakebed pockmarks in Burlington Bay, Lake Champlain: I. Hydrodyanmics and implications of origin. In: Manley, T.O., Manley, P.L. and Mihuc, T.B. (eds.), Lake Champlain: Partnerships and Research in the New Millennium. Springer, Berlin Heiderlberg New York, p. 299-330.

Manning, A.J., Baugh, J.V., Soulsby, R.L., Spearman, J.R., and Whitehouse, R.J.S., 2011, Cohesive sediment flocculation and the application to settling flux modeling. In: Silvia Susana Ginsberg (eds.), Sediment Transport. InTech, 334 p.

Mazzullo, J., Leschak, P., and Prusak, D., 1988, Sources and distribution of Late Quaternary silt in the surficial sediment of the northeastern continental shelf of the United States. Marine Geology, v. 78, p. 241-254.

McCabe, R.M., MacCready, P., and Pawlak, G., 2006, Form drag due to flow separation at a headland. Journal of Physical Oceanography. v. 36, p. 2136-2152.

Mignoit, P.C., 1968, A study of the physical properties of various ver fine sediments and their behavior under hydrodynamic action. Houille Blanche, v. 23, p. 591-620.

Mikkelsen, O.A., Milligan, T., Hill, P., Moffatt, P., 2004, INSSECT – an instrumented platform for investigating floc properties close to the bottom boundary layer. Limnology and Oceanography: Methods, v. 2, p. 226-236.

Paull, C.K., Ussler, W., Maher, N., Greene, H.G., Rehder, G., Lorenson, T., and Lee, H., 2002, Pockmarks off Big Sur, California. Marine Geology, v. 181, p. 323-335.

PEARL, 2011, Penobscot River Synthesis. http://www.pearl.maine.edu/windows/ penobscot/research_hydrology.htm

Pickrill, R.A., 2006, Shallow seismic stratigraphy and pockmarks of a hydrothermally influenced lake, Lake Rotoiti, New Zealand. Sedimentology, v. 40, p. 813-828.

Ritt, B., Pierre, C., Gauthier, O., Wenzhofer, F., Boetius, A., and Sarrazin, J., 2011, Diversity and distribution of cold-seep fauna associated with different geological and environmental settings at mud volcanoes and pockmarks of the Nile Deep-Sea Fan. Marine Biology, v. 158, p. 1187-1210.

Rockwell, D., and Naudascher, E., 1978, Review- Self-sustaining oscillations of flow past cavities. Journal of Fluids Engineering, v. 100, p. 152-165.

Rogers, J.N., Kelley, J.T., Belknap, D.F., Gontz, A., and Barnhardt, W.A., 2006, Shallow-water pockmark formation in temperate estuaries: a consideration of origins in the western gulf of Maine with special focus on Belfast Bay. Marine Geology, v. 225, p. 45-62.

Sarohia, V., 1977, Experimental investigation of oscillations in flows over shallow cavities. The American Institute of Aeronautics and Astronautics Journal, v. 15, p. 984-991.

Scanlon, K.M., and Knebel, H.J., 1989, Pockmarks in the floor of Penobscot Bay, Maine. Geo-Marine Letters, v. 9, p. 53-58.

Tennekes H., and Lumley, J.L., 1999, A First Course in Turbulence. IBM Universe Medium, United States of America, 305 p.

US Geological Survey, 2010, Stream Gauge Data, http://waterdata.usgs.gov/me/nwis

Ussler, W. III, Paull, C.K., Boucher, J., Friederich, G.E., and Thomas, D.J., 2003, Submarine pockmarks: a case study from Belfast Bay, Maine. Marine Geology, v. 202, p. 175-192.

Van Kessel, T.V., and Blom, C., 2012, Rheology of cohesive sediments: comparison between a natural and an artificial mud. Journal of Hydraulic Research, v. 36, p. 591-612.

Van Leussen, W., 1988, Aggregation of particles, settling velocity of mud flocs: a review. In: Dronkers, J., Van Leussen, W. (eds.), Physical processes of estuaries. Springer, Berlin, p. 347-403.

Weather Underground Organization, 2011, http://www.wunderground.com/

Webb, K.E., Hammer, Ø., Lepland, A., and Gray, J.S., 2009, Pockmarks in the inner Oslofjord, Norway, Geo-Marine Letters, v. 29, p. 111-124.

Wentworth, C.K., 1922, A scale of grade and class terms for clastic sediments. Journal of Geology, v. 30, p. 377-392.

Whitehouse, R., Soulsby, R., Roberts, W., and Mitchener, H., 2000, Dynamics of estuarine muds, Thomas Telford London, 210 p.

Wildish, D.J., Akagi, H.M., McKeown, D.L., and Pohle, G.W., 2008, Pockmarks influence benthic communities in Passamaquoddy Bay, Bay of Fundy, Canada. Marine Ecology Progress Series, v. 357, p. 51-66.

Winterwerp, J.C., and Van Kesteren, W.G.M., 2004, Introduction to the physical of cohesive sediment in the marine environment. Elsevier Inc., Amsterdam, 466 p.

Xue, H., and Brooks, D., 2000. Characterization of fronts and eddies in Penobscot Bay using a three-dimensional ocean circulation model. Final Report presented to Island Institute, Rockland, ME.

Xue, H., Xu, Y., Brooks, H., Pettigrew, N., and Wallinga, J., 2000, Modeling the circulation in Penobscot Bay, Maine. Estuarine and Coastal Modeling – Proceedings of the Sixth International Conference, American Society of Engineers, New Orleans, Louisiana, November 3-5, 1999.